AGU ADVANCING EARTH AND SPACE SCIENCE

Water Resources Research

RESEARCH ARTICLE
10.1029/2020WR027911

Uncertainty Analysis and Identification of Key Parameters Controlling Bacteria Transport Within a Riverbank Filtration Scenario

Dustin Knabe[1], Alberto Guadagnini[2], Monica Riva[2], and Irina Engelhardt[1]

[1]Department of Hydrogeology, Technische Universität Berlin, Berlin, Germany, [2]Dipartimento di Ingegneria Civile e Ambientale (DICA), Politecnico di Milano, Milano, Italy

Key Points:

- Inactivation, straining, and permeability of the colmation layer are key for bacteria transport at riverbank filtration sites
- Bacteria transport is markedly driven by seasonal variations of the river stage, temperature, and oxygen content
- Uncertainty linked to bacteria transport parameters is quantified via stochastic inverse modeling relying on a 1-year monitoring campaign

Supporting Information:

Supporting Information may be found in the online version of this article.

Correspondence to:

D. Knabe,
dustin.knabe@tu-berlin.de

Citation:

Knabe, D., Guadagnini, A., Riva, M., & Engelhardt, I. (2021). Uncertainty analysis and identification of key parameters controlling bacteria transport within a riverbank filtration scenario. *Water Resources Research*, *57*, e2020WR027911. https://doi.org/10.1029/2020WR027911

Received 12 MAY 2020
Accepted 24 FEB 2021

Abstract Managed aquifer recharge through bank filtration is an important method to produce sustainable drinking water. Yet, water quality related to transport of pathogens (bacteria and viruses) into groundwater systems from surface waters can be a matter of concern, especially in urbanized regions. Based on a 1-year monitoring campaign, a reactive transport model was developed for bacteria transport at a riverbank filtration site located in Germany. The model allows simulating advective-dispersive transport and relies on the colloid filtration theory to mimic attachment and detachment of bacteria to and from the sediment in addition to inactivation, straining and blocking of bacteria. Due to the complexity of the investigated processes, the reactive transport model is characterized by a high level of parametrization, encompassing parameters driving flow as well as solute and colloid transport. A global sensitivity analysis has been applied to identify the most relevant model parameters with respect to piezometric pressure heads, groundwater temperature, and concentrations of chloride, oxygen, coliforms, and *Escherichia coli*. The model has been calibrated within a stochastic framework, to provide model parameter estimates and to quantify their uncertainty. Our results suggest that bacteria transport models are highly sensitive to inactivation coefficients, straining coefficients, and bacteria size. Permeability of the colmation layer at the riverbank is a key factor for bacteria transport through its influence on residence times. Seasonal variability of boundary conditions, especially anoxic aquifer conditions in the summer and high groundwater flow velocities during flooding periods, resulted in a reduction of inactivation and increased bacteria concentrations at observation wells.

1. Introduction

Managed aquifer recharge using bank filtration is an important approach to produce sustainable drinking water in regions with limited groundwater resources. Gillefalk et al. (2018) provide an overview of the global usage of induced river bank filtration (RBF). For example, RBF provides about 60% of the total drinking water demand in the city of Berlin (Germany, 3.6 Mio. inhabitants), while it is used to serve almost 100% of the population of Düsseldorf (Germany, 0.6 Mio inhabitants) with drinking water (Gillefalk et al., 2018). The RBF concept is based on natural remediation (or attenuation), that is, on the processes occurring in groundwater (such as dispersion and biodegradation) lowering contaminant concentrations, thus reducing the need for additional treatments to obtain drinking water quality.

Pathogens, for example, viruses or some bacteria, are mainly released to the environment by wastewater discharge into streams (Xagoraraki et al., 2014). Lakes and rivers around big cities or near large urban areas are often documented to be severely polluted by pathogens, resulting in a high risk of pathogen contamination of groundwater, including RBF sites. Pathogens in drinking water can cause a variety of diseases in humans. The number of pathogen particles which are necessary to cause an infection (also termed infective dose) can vary between a few particles to thousands of particles, depending on the pathogen species (Schmid-Hempel & Frank, 2007). Accurate assessment of pathogen fate and transport are especially relevant for pathogens with a low infective dose. Bacteria concentrations serve as primary indicators for drinking water quality, as set in the World Health Organization guidelines (WHO, 2017) and regulations in several countries (e.g., EU Drinking Water Directive *98/83/EC*). Measured bacteria are either pathogens (e.g., some *Escherichia coli* strains, or the genus Enterococcus) or pathogen/wastewater indicators (e.g., coliforms).

Transport of pathogens, which can be described as bio-colloids due to their size (Hunt & Johnson, 2017), is affected by advection/dispersion processes as well as by inactivation and attachment/detachment to the solid matrix (e.g., Hunt & Johnson, 2017; Molnar et al., 2015). Inactivation is the loss of reproduction capability, which in turn is related to infectivity, and is only relevant for specific time scales. It is often negligible at laboratory scales, where residence times are typically shorter than a day (e.g., Sasidharan et al., 2017). However, the significance of inactivation increases when considering residence times associated with field scale scenarios (Kvitsand et al., 2015). Yet, the main characteristics of inactivation depend on the individual species considered, and on physical and biogeochemical conditions. In general, higher temperatures increase inactivation (e.g., de Roda Husman et al., 2009; Gordon & Toze, 2003). Additionally, Schijven et al. (2016) show that pH, as well as sodium and calcium concentration, influence inactivation of a dsDNA bacteriophage, PRD1, at the laboratory scale. Employing multiple batch experiments for *E. coli*, MS2, Poliovirus, and Coxsackievirus, Gordon and Toze (2003) document that inactivation of a given bio-colloid is markedly influenced by the activity of other microorganisms co-existing in the system. These authors conclude that other parameters, such as temperature and oxygen concentration, influence inactivation through control of the general microbiological activity. Inactivation is typically modeled as a first-order kinetics (e.g., Hornstra et al., 2018; Kvitsand et al., 2015). However, a two-rate or a bi-phasic model might be necessary for settings where inactivation is documented to decrease with time. In this latter scenario, the occurrence of such a kinetic behavior is typically due to the co-existence of two bio-colloid subpopulations (e.g., de Roda Husman et al., 2009; Schijven et al., 2016).

Macroscale description of attachment of bio-colloids should take into account the influence of mineral composition of the sediments and grain size distribution (Chrysikopoulos & Aravantinou, 2014; Mayotte et al., 2017; Park et al., 2017; Weaver et al., 2013), porosity, colloid size, flow velocity (Messina et al., 2015; Tufenkji & Elimelech, 2004), surface charge and roughness of both sediments and colloids (Argent et al., 2015), nanoscale surface heterogeneity (Johnson et al., 2018), ionic strength (Mondal & Sleep, 2013; Sasidharan et al., 2017), presence of divalent ions (Mondal & Sleep, 2013; Sadeghi et al., 2013), pH, isoelectric point of the colloid (Sasidharan et al., 2017), temperature (Chrysikopoulos & Aravantinou, 2014; Sasidharan et al., 2017), and water saturation (Chu et al., 2003; Syngouna & Chrysikopoulos, 2015).

At the pore scale, current conceptual model formulations for colloid transport include colloids transported in the bulk water phase and colloids located in the region near to the surface of the solid grains (Hunt & Johnson, 2017). In the latter case, results from a complex force and torque balance based on colloid-grain interactions and the local flow field suggests that colloids can be either immobile or mobile, also including the possibility of a return to the bulk water phase (Hunt & Johnson, 2017). Additionally, straining of colloids can occur, that is, colloids can be retained in pore throats which are too small when compared to the colloid characteristic size (Bradford et al., 2003; Johnson et al., 2007).

Macroscale transport of bio-colloids can be simulated through the colloid filtration theory (CFT). Due to negative surface charge of quartz and bio-colloids at pH $\approx$ 7, a condition which is associated with most shallow groundwater systems, unfavorable attachment conditions (attachment efficiency, α, smaller than 1) exist (Johnson et al., 2007; Sasidharan et al., 2017). This, results in repulsion between colloids and grains and the ensuing detachment of colloids to the water phase. Recent studies focusing on pathogen and bio-colloid transport at pore and laboratory scale have formed the basis for the development of improved process-based models. In this context, Hilpert and Johnson (2018) formulate a one-dimensional model which includes the presence of retarded colloid transport in the near-surface zone around grains in addition to the presence of mobile colloids in the bulk water phase and immobile colloids on grain surfaces. To the best of our knowledge, rigorous formulations for up-scaling of these pore scale modeling approaches to the continuum scale are still lacking, so that application of these concepts under highly dynamic natural field-scale conditions is still a remarkable scientific and operational challenge.

Field scale models with varying degrees of complexity have been used to simulate bio-colloid transport. Some models employ first-order inactivation and constant first-order coefficients for bio-colloid removal as a function of the transported distance. Blaschke et al. (2016) and Derx et al. (2013) model bio-colloid transport under various conditions (varying, e.g., flow velocity, porosity, and vadose zone properties) without considering the impact of hydraulic conditions on bio-colloid removal coefficients. Kvitsand et al. (2015) and Hornstra et al. (2018) consider models with increased complexity upon relying on kinetic

attachment/detachment formulations. The study of Kvitsand et al. (2015) relies on a two-site attachment model, which is explained by the presence of chemical heterogeneity, to fit observed MS2 breakthrough curves. Field scale models often cannot encompass the full process complexity of laboratory scale models or include all uncertain model parameters in the model calibration due to the high computational costs. Not all of the parameters shown to affect bio-colloid transport at laboratory scale might be relevant for the description of complex hydrological/hydrogeological systems at field scale (and vice-versa), since the relevant environmental conditions might not change strongly enough or correlating effects might be present. In this framework and given the large number of parameters required in field scale models of bio-colloid transport in porous media, our first objective is to diagnose the behavior of a field scale model of bacteria transport, as driven by uncertainties associated with its parameters prior to model calibration. We do so upon relying on a global sensitivity analysis (GSA) approach which enables us to (*a*) identify model parameters which are most influential on bacteria-sized bio-colloid transport at field scale and under natural hydraulic and geochemical conditions, as embedded in the employed model and (*b*) quantify the degree of influence of each model parameter to the variability of target model results. This approach enables us to screen model parameters on the basis of the evaluation of elementary effects and ensuing global sensitivity indices (Campolongo et al., 2007; Morris, 1991) and is preparatory to inverse modeling. The latter is performed in a probabilistic context, yielding estimates of the probability distribution of the identified influential model inputs conditional to available data.

Bio-colloid transport in natural environments is affected by variations of hydrological, hydrogeological and biogeochemical conditions often changing at seasonal or even daily time scales. Fluctuations of these environmental conditions result in a high temporal and spatial variation of many key quantities (e.g., temperature, pH, saturation, flow velocity, microbial activity, and others) that drive bio-colloid transport. Observed removal rates of bio-colloids under field conditions vary strongly over multiple orders of magnitudes (Hornstra et al., 2018; Pang, 2009; Sprenger et al., 2014). Field studies typically report lower removal rates than in laboratory scale investigations performed under similar conditions (Pang, 2009; Wielen et al., 2008). Due to low natural bio-colloid concentrations, many field studies are using an injection-based bio-colloid monitoring with short observation times and high injection concentrations. Bio-colloid transport models based on these studies are typically set-up to cover an observation period of less than a month (Hornstra et al., 2018; Kvitsand et al., 2015; Weaver et al., 2013; Wielen et al., 2008), and cannot capture all effects of seasonal variability. Therefore, an additional key objective of our study is to use the results of the stochastic model calibration to analyze bio-colloid transport across a hydrological year through the dynamics of *E. coli* and coliform bacteria. This can further help to improve our understanding of bacteria transport at facilities which provide drinking water over longer time scales (such as riverbank filtration plants).

2. Methods

2.1. Numerical Model Set-Up

Numerical investigations are conducted for a riverbank filtration site, the waterworks Flehe, located at the river Rhine in the city of Düsseldorf, Germany. The conceptual geological model (Figure 1) is based on a previous study by Sharma et al. (2012).

Extraction wells are equally spaced in a highly permeable sand-gravel aquifer in 20 m intervals parallel to the river and at a distance of 80 m to the river. We investigated a simplified two-dimensional transect (Figure 1), which contains the multi-level observation well B, the extraction well Q, and groundwater well G. The transect is perpendicular to the river and three-dimensional flow effects were observed to be negligible justifying a two-dimensional approach. Observation well B is characterized by 3 screened intervals (1 m length, located at 19 m (B1), 23 m (B2), and 26 m (B3) a.s.l., Figure 1). Our investigation includes the analysis of measurements of pathogen indicator bacteria, *E. coli* and coliform bacteria, collected between January 2003 and March 2004 (440 days). In situ measurements of piezometric pressure head, temperature, and oxygen concentration were taken during this period between once and twice per week. Analyses of target species (Na^+, K^+, Ca^{2+}, Mg^{2+}, Cl^-, NO_3^-, SO_4^{2-}) were also performed through ion-chromatography at a bi-weekly interval. Water samples were also collected every 2 weeks for detection of bacteria and analyzed with plate growth test according to DIN EN ISO 9308-2. All samples were collected from well B (at depths corresponding to B1, B2, and B3), Q, and G as well as from the river Rhine.

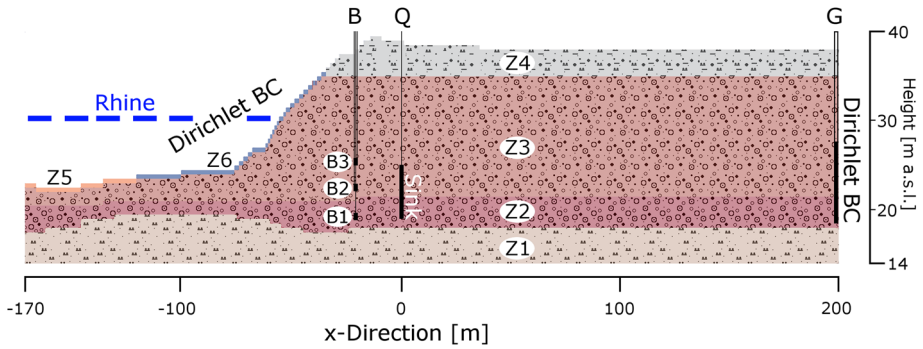

Figure 1. Sketch of the hydrogeological model, including zonation and wells. Zones/layers are identified as: Z1, Aquitard (silty fine sand); Z2, Lower Aquifer (Sand-Gravel); Z3, Upper Aquifer (Sand-Gravel); Z4, Soil Zone (silty clayey sand); Z5, river bed (sand-gravel with very light clogging); and Z6, Colmation Layer (strongly silt clogged sand-gravel). Identifiers B and G are associated with observation wells, Q denoting the extraction well. B1, B2, and B3 further denote the different levels of well B.

We perform flow and transport simulations within the two-dimensional domain depicted in Figure 1 via the numerical open-source code PFLOTRAN (Lichtner et al., 2019). To simulate subsurface flow and transport of thermal energy we employ PFLOTRAN's *TH-mode* ("*T*hermal-*H*ydrologic"), which solves the fully coupled system of fluid mass and energy conservation equations. Reactive transport processes are implemented via the PFLOTRAN's *Reaction Sandbox*. A single model run used one computation node (2 × 12 CPU cores Intel Xeon IvyBridge @2.4 GHz or Intel Xeon Haswell @2.5 GHz) and required 4–5 min runtime.

2.2. Groundwater Flow and Conservative Transport Model

Bacteria transport is simulated along the two-dimensional domain depicted in Figure 1. Flow is assumed to be two-dimensional due to the constant pumping, and the regular distances between the extraction wells and the river. The domain is characterized by a horizontal length of 370 m and a height of 26 m. A uniform discretization is applied along the vertical direction (i.e., along the z-axis) with a discretization interval $dz = 0.5$ m. Horizontal discretization, dx, is equal to 1 m in the region comprised between the middle of the river Rhine (at $x = -170$ m) and the zone close to the riverbank (at $x = +30$ m). A stepwise increasing discretization is applied for 30 m $< x \leq$ 200 m (with $dx = 2$ m for 30 m $< x \leq$ 40 m and $dx = 5$ m for 40 m $< x \leq$ 200 m), thus resulting in a total number of 225 × 52 cells.

The extraction well (Q in Figure 1) is simulated with a time-variable extraction rate. The well screen (total length 7 m, i.e., 14 cells) extends over the two aquifer layers (Z2 and Z3). Output values for target variables at Q were calculated by using a permeability-based weighted average of the model outputs at the screen cells. The screened intervals of well B are discretized with three cells. Here, output values for target variables are calculated by using a weighted average of values obtained for the three model cells based on the fraction of the overlap between the well screen and the three model cells, as the vertical position of the well screen does not (generally) align with the numerical grid considered. Time dependent Dirichlet boundary conditions are used (*i*) at the river (along the upper face of the cells comprising the river bed and the colmation layer, Z5 and Z6) and (*ii*) at the landside (along the right face of the outermost cells, $x = 200$ m). Values employed for these boundary conditions are included in Section 3.1 (for the river boundary) and in Figure S1 (for the landside groundwater boundary). The remaining boundaries (at $x = -170$ m and at $z = 14$ m) are set as no flow.

A spin-up period of 60 days is defined prior to the main simulation focused on the data collection period to obtain an initial distribution for the model variables (piezometric pressure heads, temperature, chloride, oxygen, dissolved organic carbon [DOC], and bacteria concentrations). For this period, boundary condition values for model variables correspond to the first available measurement at the boundary. The length of 60 days for the spin-up period guaranteed attaining approximately steady-state conditions across the domain for the target output variables, with the aim of minimizing the effects of the selected initial condition values. The total simulation time is 500 days, including the 60-day spin-up period. Computations rely on the stand-

ard adaptive time-stepping of PFLOTRAN with an initial time step of 0.01 d, a maximum time step of 0.5 d, and forced output times every 0.5 d. Values defined for piezometric pressure heads, temperature, chloride, oxygen, and DOC as boundary conditions were interpolated linearly from the collected data, a log-linear interpolation being used for *E. coli* and coliforms. The interpolation enables us to project the measurements to a 0.5-day time step to match the output times. Day 60 of model simulations corresponds to 01.01.2003.

A constant (yet unknown) value for longitudinal dispersivity, δ_L, is considered (anisotropy is tackled by introducing the ratio $\delta_{\text{aniso}} = \delta_L/\delta_T$, δ_T being transverse dispersivity), while porosity, n_{Zi}, and permeability, $K_{p,Zi}$ (with $i = 1,...6$) vary across the zoned model domain. Permeability and porosity for zone Z1 (aquitard, silty fine sand) are defined based on the classification of core samples collected during well drilling. We set a porosity $n_{Z1} = 0.2$ and a permeability $K_{p,Z1} = 5 \times 10^{-12}$ m^2 for zone Z1, while permeability and porosity parameters for zones Z2–Z6 are unknown and estimated via Stochastic calibration.

Permeability for zones Z2 (lower aquifer), Z3 (upper aquifer), and Z5 (river bed) is evaluated via the Kozeny-Carman equation (Carrier, 2003) on the basis of available grain sieve analyses as:

$$K_{p,Zi} = \frac{1.99}{S_0^2}\left(\frac{n_{Zi}^3}{1+n_{Zi}}\right) \tag{1}$$

$$S_0 = \frac{1}{\text{SF}}\sum_j \frac{f_j}{D_{lj}^{0.404} D_{sj}^{0.595}} \tag{2}$$

where S_0 is the specific surface area per unit volume of particles [m^{-1}]; SF is a shape factor (here set as SF = 6.6, since solid particles are mostly rounded; Carrier, 2003); f_j is the fraction of particles retained on sieve j [-], D_{lj} *and* D_{sj} being the largest and smallest particle size on sieve j [m], respectively. We also consider anisotropy, as expressed through an anisotropy ratio ($K_{\text{aniso}} = K_x/K_z$).

Permeability of the colmation layer (Z6) can vary over orders of magnitude over a hydrological year due to variability of precipitation, stream discharge, sediment loads, or biogeochemical activity (Hatch et al., 2010; Schubert, 2002; Zhou et al., 2018). To include this feature in our model, we subdivide the temporal window of our simulations into five time periods. These are characterized by three main events, each separated by an intermediate period. In details, the five defined temporal periods (TPj; $j = 1, ..., 5$) are: TP1 (days 0–80)—corresponding to an initial flood event observed at the beginning of the observation period; TP2 (days 80–220)—intermediate period; TP3 (days 220–300)—summer period, with low discharges and high temperatures; TP4 (days 300–435)—intermediate period; and TP5 (days 435–500)—second flood event.

For thermal properties, the subsurface zones were divided into aquifer (sand-gravel; Z2, Z3) and non-aquifer (fine sand-silt; Z1, Z4, Z5, Z6). Each of the two classifications were assigned a single parameter for heat capacity C and thermal conductivity $\varkappa$.

2.3. Implemented Reaction Network

A broad set of kinetic reactions are implemented in our bacteria transport model. We consider attachment to the sediment through CFT and the Maxwell approach to calculate the collision efficiency, α, from the DLVO (Derjaguin-Landau-Verwey-Overbeek) interaction energies (Shen et al., 2007). Detachment, straining, blocking, and inactivation are also implemented (Bradford et al., 2003; Kvitsand et al., 2015; Sadeghi et al., 2013; Wang et al., 2013). For inactivation, dependence on oxygen concentration is included, which additionally leads to the inclusion of aerobic respiration as main reactive process for oxygen variation in the subsurface.

2.3.1. Aerobic Respiration

Oxygen consumption by sediment organic carbon (SOC) and DOC degradation is implemented in way similar to Sharma et al. (2012):

$$CH_2O + O_2 \rightarrow CO_2 + H_2O \tag{3}$$

$$r_{\mathrm{SOC}} = f_T \left[k_{\mathrm{SOC}} \left(\frac{c_{O2}}{K_{\mathrm{O2,SOC}} + c_{O2}} \right) \right] \tag{4}$$

$$r_{\mathrm{DOC}} = f_T \left[k_{\mathrm{DOC}} \left(\frac{c_{O2}}{K_{\mathrm{O2,DOC}} + c_{O2}} \right) \right] \tag{5}$$

$$f_T = \exp\left(\beta T \left(1 - 0.5 \frac{T}{T_{\mathrm{opt}}} \right) \right) \tag{6}$$

where, r_j and k_j (j = SOC, DOC) are the SOC and DOC oxidation rates [mol L^{-1} s^{-1}] and the corresponding rate constants [mol L^{-1} s^{-1}], respectively; c_{O2} is the concentration of dissolved oxygen [mol L^{-1}]; $K_{O2,j}$ (j = SOC, DOC) is the half saturation constant for dissolved oxygen [mol L^{-1}]; f_T is a factor including temperature effects on reaction rates [−]; β is a model parameter mainly influencing the rate of change of f_T with temperature [$°C^{-1}$]; T is temperature [°C]; and T_{opt} is the temperature at which the reaction rate is fastest [°C].

It is assumed that SOC as electron donor is unlimited in our timeframe, that is, SOC consumption does not impact SOC oxidation rates. In the absence of SOC measurements and considering limited availability of spatial observations for DOC, we take SOC to be homogeneously distributed in space. As suggested by Sharma et al. (2012), we note that considering this approach in an inverse modeling context tends to be conducive to underestimated values of the SOC oxidation rate constant, as opposed to considering a higher concentration/reactivity of SOC close to the river. SOC oxidation is assumed to be direct, without emergence of DOC as intermediate product. Due to a residual DOC concentration of about 8×10^{-5} mol L^{-1} (2.4 mg/L, assumed as CH_2O), which was observed in the observation wells (see Figure 2 in Section 3), a threshold value for DOC is defined below which DOC oxidation does not take place. We note that we employed the Monod rate formulation for organic carbon degradation similar to Sharma et al. (2012), who previously modeled oxygen depletion based on the current data set. Considering a more complex formulation, as used in, for example, Dwivedi et al. (2018), will likely not enhance the model results due to the limited amount of data and the fact that bacteria transport is coupled with oxygen and not DOC concentration.

2.3.2. Bacteria/Colloid Transport

Bacteria transport considers attachment to and detachment from the sediment, inactivation, as well as straining and blocking. Attachment, detachment, and inactivation are implemented as first-order kinetics (e.g., Sadeghi et al., 2013).

The attachment coefficient is calculated according to the CFT (Sadeghi et al., 2013):

$$k_{\mathrm{att}} = \frac{3\left(1 - \theta_w\right)}{2\, d_g} v\, \eta\, \alpha \tag{7}$$

where θ_w is volumetric water content [−], d_g is an (effective) grain diameter [m]; v is fluid velocity [m s^{-1}]; and η and α are the collision [−] and the attachment [−] efficiency, respectively. Following Messina et al. (2015), a total flux normalized equation is employed to calculate η (supporting information Text S1), this strategy providing better results under very low flow velocities as compared to previous models (Messina et al., 2015). A few additions to the PFLOTRAN source code to enable the fluid velocity as a parameter in the reaction sandbox can be found at https://bitbucket.org/dknabe/pflotran-darcy-velocity-in-reaction-sandbox/branch/dustin/darcy-velocity-in-reaction-sandbox.

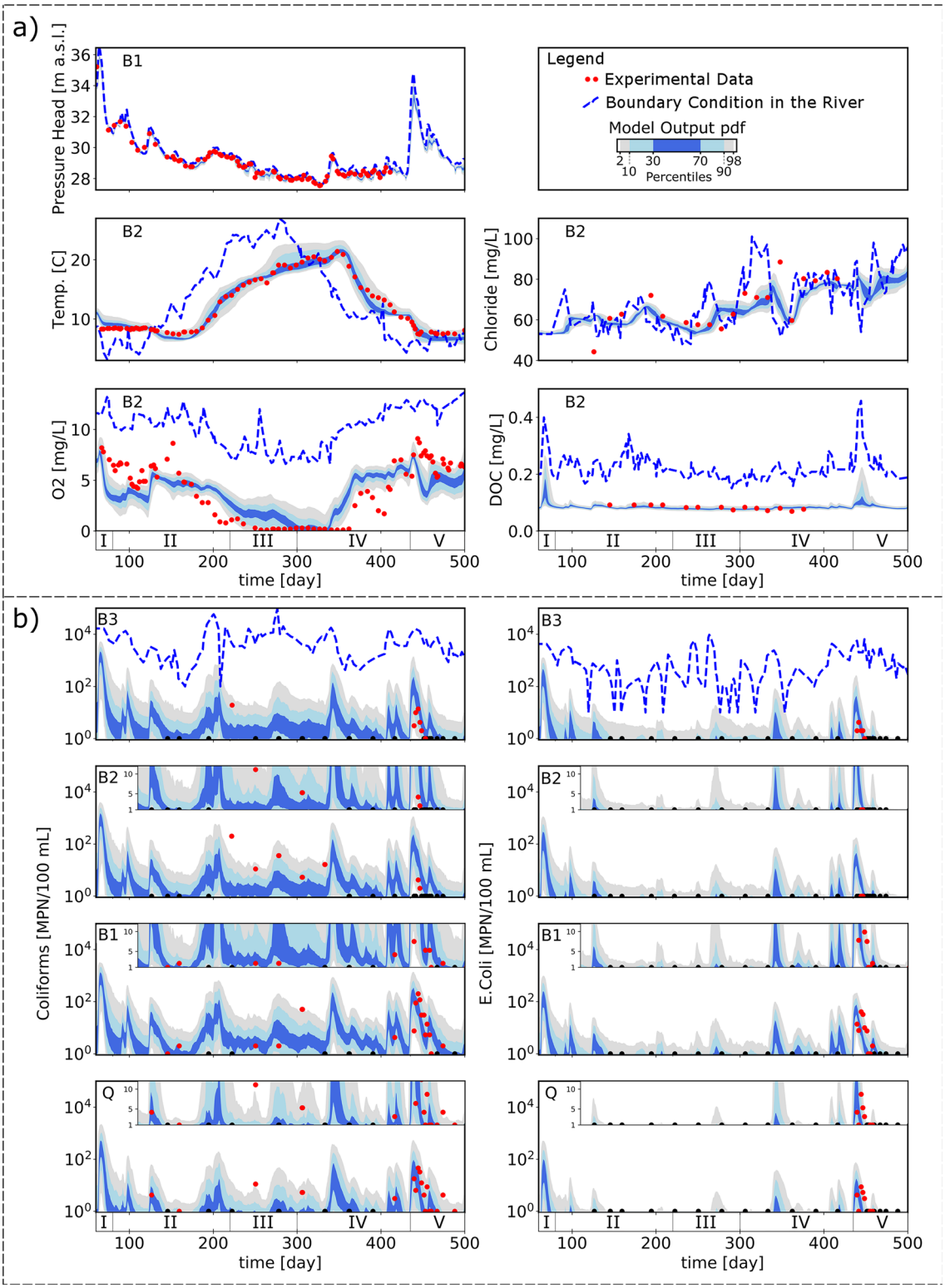

Figure 2. Measured data and stochastic model calibration outputs versus time for (a) piezometric pressure head (well B, location B1), conservative solute, heat transport, and organic carbon respiration (well B, location B2), and for (b) coliform and *E. coli* concentrations at all well B locations and extraction well Q. Temporal periods (TP I to V) of the simulation and the colmation layer permeability (I to V) are marked on the horizontal axis. Shaded areas represent the output variability of the 375 PSO-based solutions through selected percentiles of the empirical output probability distribution. Insets in (b) for well Q and locations B1 and B2 of well B complement the results by focusing on the smallest concentration values (in the range 1–10 MPN/100 mL) represented on a linear scale for the vertical axis.

The attachment efficiency α describes the probability for a colloid to attach to surfaces after collision. CFT was originally derived on the basis of favorable conditions for attachment (attachment efficiency $\alpha = 1$) but has also been applied successfully in numerous studies for unfavorable attachment conditions, where $\alpha < 1$ (Kvitsand et al., 2015; Sadeghi et al., 2013; Schijven et al., 2002). We employ the Maxwell Approach (e.g., Shen et al., 2007), which accounts for the DLVO interaction energy curve between the colloid and the sediment surface. The Maxwell Approach relies on the assumption that the probability of attachment can be evaluated through a Maxwell distribution for the kinetic energy of the colloids. The formulation of the DLVO in our model relies on the Sphere-Sphere Geometry with the model for Van-der-Waals forces of Gregory (1981), electrostatic double layer forces of Hogg et al. (1966), and born repulsion of Feke et al. (1984) (supporting information Text S2). Ionic strength, which is used in the DLVO calculation, varied only slightly within the model domain (in the data between 0.008 and 0.012 mol L^{-1}). However, as the available data did not allow to properly include the main hydrochemical species in the model, IS_{HOM} is considered as an uncertain parameter in our modeling approach. Furthermore, pH, which could affect colloid and mineral surface charges, remains almost constant during the investigated period, and varied between 7.2 and 7.8 in the groundwater. This minimal variation is not strong enough to significantly affect bacteria transport, as both quartz sand and bacteria such as *E. coli* maintain negative surface charges even at around pH 6 (Chen & Walker, 2007; Wang et al., 2013).

An additional key process to be considered is inactivation. According to Gordon and Toze (2003), if additional microorganisms are present, availability of oxygen can influence inactivation of bacteria and viruses. During the first months of field investigations, aerobic conditions occurred with a transition to anoxic conditions (c_{O2} <10 μmol L^{-1}) from day 250 to day 362. During these anoxic conditions, that were linked to low flow velocities and high groundwater temperature, a breakthrough of coliforms was observed at the monitoring locations. Based on this observation, we include inactivation as depending on dissolved oxygen concentration, c_{O2} [mol L^{-1}], as:

$$k_{\text{inac},m/im,i}\left(c_{O2}\right) = \begin{cases} k_{\text{inac},m/im,i} & , c_{O2} \geq c_{O2,\text{Threshold}} \\ f_{\text{anoxic},m/im,i}\, k_{\text{inac},m/im,i} & , c_{O2} < c_{O2,\text{Threshold}} \end{cases} \tag{8}$$

where $k_{\text{inac},m/im,i}$ is the inactivation coefficient of species i in the mobile/immobile (m/im) phase under oxic conditions [d^{-1}]; $f_{\text{anoxic},m/im,i}$ is the ratio between the inactivation coefficients at anoxic and oxic conditions in the mobile/immobile (m/im) phase for species i [−]; and $c_{O2,\text{Threshold}}$ is a threshold concentration [mol L^{-1}].

Straining is implemented following Bradford et al. (2003) and blocking following Wang et al. (2013), leading to:

$$-\left.\frac{\partial c_i}{\partial t}\right|_{\text{reaction}} = r_{c_i} = f\left(S\right) k_{\text{att}}\, c_i - k_{\text{det}}\, S_i - k_{\text{inac},m,i}\left(c_{O2}\right) c_i - k_{\text{str}} \left(\frac{d_{p_i}}{d_g}\right)^{p_{\text{str}}} c_i \tag{9}$$

$$-\frac{\partial S_i}{\partial t} = r_{S_i} = -f\left(S\right) k_{\text{att}}\, c_i + k_{\text{det}}\, S_i - k_{\text{inac},im,i,}\left(c_{O2}\right) S_i \tag{10}$$

$$f\left(S\right) = \frac{S_{\max} - \sum_i S_i}{S_{\max}} \tag{11}$$

where, c_i [Nr L^{-1}] and S_i [Nr L^{-1}] are concentration of bacteria i in the water and on the solid phase (evaluated as number of bacteria, Nr, per unit volume of solute for both water and solid phase concentrations), respectively; r_{ci} is the rate of change of bacteria concentration [Nr L^{-1} d^{-1}]; k_{att} and k_{det} [d^{-1}] are the attachment and detachment coefficients, respectively; $f(S)$ is the blocking coefficient [−]; $S_{\max}$ is the largest concentration that can be attached to the solid phase [Nr L^{-1}]; k_{str} is the straining coefficient [d^{-1}]; d_{p_i} is the effective size of bacteria i [m]; d_g is an effective grain size [m]; and p_{str} is the straining exponent [−]. This blocking formulation considers competition of multiple bacteria species for the same attachment locations. We note that other bacteria species are typically present in a natural system in addition to *E. coli* and coli-

forms, and all of these would compete for the same attachment locations. Additionally, colloids trapped by straining can be remobilized by a reversal of the flow direction. As the general flow is directed from the river to the extraction well Q, we consider straining as irreversible (Hunt & Johnson, 2017).

Two bacteria species are simulated: (*a*) *E. coli* and (*b*) coliforms without *E. coli*. As *E. coli* is part of the non-taxonomical group *coliforms*, we subtracted the sampled *E. coli* concentrations from total coliform concentrations to obtain concentration values for two distinct aqueous species. This enabled us to evaluate the blocking process (Equations 9–11) for both species. Note that "coliforms without *E. coli*" is termed as coliforms in the following for simplicity.

2.4. Global Sensitivity Analysis

Sensitivity analysis allows quantifying the impact of model input parameters on model results. It can be used to enhance our understanding of model functioning, which can be critical in the presence of a high dimensionality of the model parameter space, especially with regard to model calibration and models involving multiple processes with complex feedbacks. Our reactive transport model contains 59 parameters, which we treat as uncertain (Table 1 and Table S1). Model parameters are grouped with respect to the process they drive, that is, (*i*) flow and heat transport, (*ii*) dispersive transport, (*iii*) organic carbon respiration, and (*iv*) bacteria transport.

We identify parameters with a low impact on our model results by using a parameter screening method based on the evaluation of the Morris sensitivity indices (Morris, 1991). As shown, for example, by Porta et al. (2018), who relied on these indices for the analysis of a complex reaction network of atrazine biodegradation in soil, this approach is suitable when the number of uncertain parameters is high and model simulations have a high computational cost. This technique relies on the evaluation of a set of local sensitivities, typically termed as elementary effects (EEs), yielding the global sensitivity index:

$$\mu^*_{j,k}\left(\boldsymbol{x},t\right) = \frac{1}{N}\sum_{i=1}^{N}\left|\frac{df_k\left(\boldsymbol{x},t\right)}{dp_j}\right|_i \tag{12}$$

Here, $\mu^*_{j.k}\left(\boldsymbol{x},t\right)$ is the Morris sensitivity index for (normalized) parameter p_j and model output $f_k\left(\boldsymbol{x},t\right)$ at position vector $\boldsymbol{x}$ in the domain and observation time t for target variable k; $\left|df_k\left(\boldsymbol{x},t\right) / dp_j\right|_i$ is the absolute value of the ith EE associated with parameter p_j and corresponding to the rate of change of $f_k\left(\boldsymbol{x},t\right)$ due to a given increment of parameter p_j in the parameter space; and N is the number of EEs considered.

A collection of N EEs is evaluated for each model parameter by sampling random realizations of the parameter vector across the parameter space. Here, we consider model parameters to be independent and identically distributed (iid) random variables, each characterized by a uniform probability density function (Table S1). The range of parameter variability is based on prior knowledge obtained from previous site investigations and literature review. Parameter values spanning several orders of magnitude are log-transformed prior to normalization and inclusion in the sensitivity analysis procedure. Note that we assumed the variability range selected for coliform parameters to equal the one for *E. coli* parameters. This choice is based on the fact that *E. coli* is part of the non-taxonomical group *coliforms* and published experimental laboratory studies focus only on one or a few specific bacteria species, such as, for example, *E. coli*. The key purpose of our sensitivity analysis is (*i*) improving our understanding of the behavior of the considered model for all target variables (piezometric pressure head, temperature, and concentrations of chloride, oxygen, DOC, coliforms and *E. coli*) by assessing the relevance of each model parameter for each model output, and (*ii*) identifying parameters whose uncertainty does not significantly impact model results. Model parameters are treated as statistically independent since the amount of information available does not enable us to identify correlations among them. Our choice of using a uniform probability density function to characterize the uncertain model parameters relies on the idea of assigning equal weights to each value within the parameter range. This is a typical approach when information on the considered parameters and on possible degrees of cross-correlations amongst them are limited (others studies relying on the same assumption include, for example, Bianchi Janetti et al. [2019], Ciriello et al. [2013], Laloy et al. [2013], Sochala and Le Maître [2013]).

Table 1
Uncertain Model Parameters Considered in the Sensitivity Analysis (References Are Given in S1)

Parameter		Units	Uncertainty range	Log	Parameter		Units	Uncertainty range	Log
1*	$S_{0,Z2}$	m^{-1}	[5,823, 21,411]	N	31	$f_{anoxic,im,CF}$	–	[1.E-02, 1]	Y
2*	$S_{0,Z3}$	m^{-1}	[5,823, 21,411]	N	32*	$k_{det,CF}$	d^{-1}	[1.E-04, 500][d,e,i,j]	Y
3*	$K_{p,Z6,I}$	m^2	[1.E-14, 1.E-10]	Y	33*	d_{CF}	m	[1.E-05, 1.E-07][k]	Y
4*	$K_{p,Z6,II}$	m^2	[1.E-14, 1.E-10]	Y	34	ρ_{CF}	kg/m^3	[1,050, 1,150][l]	N
5*	$K_{p,Z6,III}$	m^2	[1.E-14, 1.E-10]	Y	35	A_{CF}	J/(kg K)	[5.E-22, 1.E-20][m,n,o]	N
6*	$K_{p,Z6,IV}$	m^2	[1.E-14, 1.E-10]	Y	36	ψ_{CF}	V	[−0.07, −0.0064][m,p,q,r]	N
7*	$K_{p,Z6,V}$	m^2	[1.E-14, 1.E-10]	Y	37*	$k_{inac,m,EC,oxic}$	d^{-1}	[1.E-03, 5][d,e,f,g,h]	Y
8	$S_{0,Z5}$	m^{-1}	[5,823, 21,411]	N	38*	$k_{inac,im,EC,oxic}$	d^{-1}	[1.E-03, 5]	Y
9	$K_{p,Z4}$	m^2	[1.E-13, 1.E-10]	Y	39	$f_{anoxic,m,EC}$	–	[1.E-02, 1][h]	Y
10	K_{aniso}	–	[1, 100]	Y	40	$f_{anoxic,im,EC}$	–	[1.E-02, 1]	Y
11	$C_{aquifer}$	J/(kg K)	[700, 1,000][a,b]	N	41*	$k_{det,EC}$	d^{-1}	[1.E-04, 500][d,e,i,j]	Y
12	$C_{non\text{-}aquifer}$	J/(kg K)	[700, 1,500][a,b]	N	42*	d_{EC}	m	[1.E-05, 1.E-07][k]	Y
13	$\kappa_{aquifer}$	W/(m K)	[1.5, 4][a,b]	N	43	ρ_{EC}	kg/m^3	[1,050, 1,150][l]	N
14	$\kappa_{non\text{-}aquifer}$	W/(m K)	[1.5, 4][a,b]	N	44	A_{EC}	J	[5.E-22, 1.E-20][m,n,o]	N
15*	n_{Z2}	–	[0.05, 0.4]	N	45	ψ_{EC}	V	[−0.07, −0.0064][m,p,q,r]	N
16*	n_{Z3}	–	[0.05, 0.4]	N	46*	$d_{g,Z2}$	m	[2.1E-04, 9.5E-03]	N
17	n_{Z5}	–	[0.05, 0.4]	N	47*	$d_{g,Z3}$	m	[2.1E-04, 9.5E-03]	N
18	n_{Z6}	–	[0.05, 0.2]	N	48	$d_{g,Z5}$	m	[2.1E-04, 9.5E-03]	N
19	n_{Z4}	–	[0.05, 0.2]	N	49	$d_{g,Z6}$	m	[2.E-06, 6.3E-05][s]	N
20*	δ_L	m	[1, 50]	N	50	$d_{g,Z4}$	m	[2.E-06, 6.3E-05]	N
21*	δ_{aniso}	–	[1, 100]	Y	51	ψ_g	V	[−0.083, −0.0042][m,p,r,t]	N
22*	k_{SOC}	mol/(L s)	[2.2E-13, 2.2E-11][c]	Y	52	σ_{born}	m	[2.E-10, 9.E-10][t,u]	N
23	$K_{O2,SOC}$	mol/L	[1.E-06, 1.E-04][c]	Y	53	λ_{vdw}	m	[5.E-08, 1.5E-07][u]	N
24	k_{DOC}	mol/(L s)	[2.2E-11, 2.2E-09][c]	Y	54*	$S_{max,aq}$	Nr/m^3	[0.001, 100][m,p]	Y
25	$K_{O2,DOC}$	mol/L	[3.E-05, 3.E-03][c]	Y	55	$S_{max,fl}$	Nr/m^3	[0.1, 100]	Y
26*	β	1/°C	[0.03, 0.32][c]	N	56*	k_{str}	d^{-1}	[0.005, 50][v]	Y
27	T_{opt}	°C	[30, 40][c]	N	57*	p_{str}	–	[1.0, 2.0][v]	N
28*	$k_{inac,m,CF,oxic}$	d^{-1}	[1.E-03, 5][d,e,f,g,h]	Y	58	IS_{hom}	mol/L	[0.008, 0.012]	N

Table 1
Continued

Parameter		Units	Uncertainty range	Log	Parameter		Units	Uncertainty range	Log
29*	$k_{\text{inac},im,\text{CF,oxic}}$	d^{-1}	[1.E-03, 5]	Y	59	$co_{2,\text{Threshold}}$	mol/L	[3.1E-06, 1.3E-04]	N
30	$f_{\text{anoxic},m,\text{CF}}$	–	[1.E-02, 1][h]	Y					

Note. Most sensitive parameters (MSP) resulting from the sensitivity analysis are marked with *. Parameter grouping with respect to the processes they drive is denoted by colors. Log-transformation prior to normalization denoted by "Y", no log-transformation by "N."
[a]Stauffer et al. (2013). [b]Bayer et al. (2015). [c]Sharma et al. (2012). [d]Feighery et al. (2013). [e]Schijven et al. (2013). [f]Blaustein et al. (2013). [g]Foppen et al. (2008). [h]Gordon and Toze (2003). [i]Park et al. (2017). [j]Levy et al. (2007). [k]Gerardi and Zimmerman (2005). [l]Lewis et al. (2014). [m]Wang et al. (2013). [n]Brown and Jaffé (2006). [o]Redman et al. (2004). [p]Bradford et al. (2015). [q]Li et al. (2015). [r]Chen and Walker (2007). [s]Schubert (2002). [t]Sasidharan et al. (2017). [u]Syngouna and Chrysikopoulos (2015). [v]Bradford et al. (2003).

We follow Porta et al. (2018) and rely on 50 trajectories in the parameter space (which corresponds to 3,000 model runs), the evaluation of the Morris sensitivity indices being therefore based on $N = 50$ EEs. The indices are calculated for target variables (piezometric pressure head, temperature, and concentrations of chloride, oxygen, DOC, coliforms and *E. coli*) at four locations (corresponding to extraction well Q and the three screens for observation well B) and with a temporal resolution of 12 h between days 61 and 500 giving 3,520 sensitivity indices per parameter and target variable. Note that, with reference to bacteria, we consider the logarithm of concentrations for coliform and *E. coli* as model output $f_k(\boldsymbol{x},t)$, since their concentrations vary by up to 4 orders of magnitude and are deemed as equally relevant at low and high values.

2.5. Stochastic Model Calibration

Model calibration is performed within a stochastic framework. While a deterministic inverse modeling approach aims at finding a unique set of model parameters that minimizes a given objective function, inverse stochastic modeling is intrinsically linked to the non-uniqueness of the inverse problem. In such a framework, one considers multiple possible solutions which can then be employed to fully characterize parameter uncertainty conditional to available information and to eventually provide predictions under uncertainty. The latter is quantified in terms of the probability distribution of model parameters conditioned on available information.

We implement a stochastic inverse modeling workflow by relying on the particle swarm optimization (PSO) machine-learning technique (e.g., Robinson & Rahmat-Samii, 2004). The latter is based on a stochastic evolutionary algorithm that has been shown to be conducive to robust results and with acceptable computational costs in the context of several environmental applications associated with a high number of parameters (see, e.g., Castagna and Bellin [2009], Majone et al. [2012], Russian et al. [2019] and references therein). In the PSO approach, a set of particles are initially spread randomly across the parameter space, each with an initial random velocity. The first iteration begins with the evaluation of a pre-defined objective function for each particle. The velocity of each particle is then updated depending on current and previous values of the objective function of the single particle as well as of all particles. Particles are then displaced according to their updated velocities and the algorithm continues with the next iteration until a satisfactory value of the objective function is attained.

As stochastic inverse methods tend to be computationally intensive, we rely on the GSA results to identify a reduced set of model parameters (termed most sensitive parameters, MSP) upon which the stochastic inversion is performed. To quantify the sensitivity of model parameters, we introduce the following quantity:

$$\hat{\mu}^*_{j,k} = \max_{\boldsymbol{x}\in X_k}\left[\tilde{\mu}^*_{j,k}(\boldsymbol{x})\right] = \max_{\boldsymbol{x}\in X_k}\left[\underset{t}{\text{Median}}\left(\mu^*_{j,k}(\boldsymbol{x},t)\right)\right] \tag{13}$$

where, $\tilde{\mu}^*_{j,k}(\boldsymbol{x})$ is the median (over time) of $\mu^*_{j,k}(\boldsymbol{x},t)$ at location $\boldsymbol{x}$ defined in Equation 12; and $\hat{\mu}^*_{j,k}$ is the highest value of $\tilde{\mu}^*_{j,k}(\boldsymbol{x})$ at all locations in the set X_k, which encompasses all observation points, where data

for target variable k is available. In general, X_k corresponds to {B1, B2, B3, Q} except for piezometric pressure head, where X_k corresponds solely to {B1}.

As permeability of the colmation layer Z6 varies with time, we introduce five parameters for the five different periods ($K_{p,Z6,i}; i = \mathrm{I}, ..., \mathrm{V}$), as described in Section 2.2. Note that the median of $\mu^*_{j,k}(\boldsymbol{x},t)$ would possibly underestimate the sensitivity of $K_{p,Z6,i}$, as each of these five parameters is only active during a specific period. Thus, we lump all values of $\mu^*_{j,k}(\boldsymbol{x},t)$ and consider a representative index evaluated as:

$$\mu^*_{\{3-7\},k}(\boldsymbol{x},t) = \sum_{j\in\{3-7\}} \mu^*_{j,k}(\boldsymbol{x},t) \tag{14}$$

where $j \in \{3-7\}$ corresponds to the parameter identifying number of the colmation layer permeability (Table 1). Therefore, $\mu^*_{\{3-7\},k}(\boldsymbol{x},t)$ is a representative Morris index (evaluated at location $\boldsymbol{x}$ and time t) summarizing the influence (on the target output k) of the permeability of the colmation layer across all periods.

The parameter set MSP is then used in the stochastic model calibration phase. Selection of MSP is achieved by ordering parameters for each target variable based on the associated value of $\hat{\mu}^*_{j,k}$. For a given target variable, a subset MSP_k is identified by ordering $\hat{\mu}^*_{j,k}$ in descending order and adding parameters to MSP_k until the following condition is satisfied:

$$\mathrm{MIR}_k = \frac{\sum_{j\in \mathrm{MSP}_k} \hat{\mu}^*_{j,k}}{\sum_j \hat{\mu}^*_{j,k}} > \begin{cases} 50\% \text{ if } k \text{ is neither Coliforms nor } E.\,coli \\ 70\% \text{ if } k \text{ is either Coliforms or } E.\,coli \end{cases} \tag{15}$$

Here, MIR_k (Morris Index Ratio) is the ratio of the sum of the sensitivity indices included in MSP_k with respect to the total sum of the sensitivity indices. The set of MSP used in the stochastic model calibration is formed by merging of all subsets MSP_k for all target variables. The remaining parameters (not included in MSP) were set equal to the central value of the corresponding parameter range used in the sensitivity analysis (Table S1).

The objective function to be minimized in the stochastic model calibration embeds measured observations for piezometric pressure heads, temperature, as well as chloride, oxygen, DOC concentration and logarithm values of *E. coli* and coliforms concentration. The contribution, ϕ_k, of the target variable k to the objective function is evaluated as:

$$\phi_k = \frac{1}{N_k}\left(\sum_{\boldsymbol{x}}\left(\sum_t\left(\frac{f_{m,k}(\boldsymbol{x},t) - f_{o,k}(\boldsymbol{x},t)}{\max\limits_{\boldsymbol{x},t} f_{o,k} - \min\limits_{\boldsymbol{x},t} f_{o,k}}\right)^2\right)\right) \tag{16}$$

where $f_{m,k}(\boldsymbol{x},t)$ is the model output and $f_{o,k}(\boldsymbol{x},t)$ the observed value of target variable k at location $\boldsymbol{x}$ and time t; $\max_{\boldsymbol{x},t} f_{o,k}$ and $\min_{\boldsymbol{x},t} f_{o,k}$ are the maximum and minimum values of $f_{o,k}(\boldsymbol{x},t)$, respectively. To include observations with no detections for *E. coli* and coliforms (actual concentrations below the detection limit) in this procedure, model outputs below the limit and observed values corresponding to a sample analysis with no detection of *E. coli* or coliforms were set to the logarithm of the detection limit value of 1 MPN/100 mL.

The total objective function, ϕ_{tot}, during each PSO iteration is then evaluated as:

$$\phi_{\mathrm{tot}} = \sum_k \log_{10}(\phi_k) \tag{17}$$

to ensure that each component has an impact on the overall optimization process.

The PSO is implemented using 30 particles (points at which the objective function value is calculated) and 30 displacements (iterations at which objective function values are calculated). The number of par-

ticles and displacements were selected as a compromise between convergence success rate and computational efforts required. Velocity update between displacements is calculated according to Robinson and Rahmat-Samii, 2004:

$$v_{i,j,m} = \omega_m v_{i,j,m-1} + 1.495\,\mathrm{rand}\left(p\mathrm{best}_{i,j} - p_{i,j}\right) + 1.495\,\mathrm{rand}\left(g\mathrm{best} - p_{i,j}\right) \quad (18)$$

$$\omega_m = 0.9 - 0.5\frac{m}{m_{\max}} \quad (19)$$

where $v_{i,j,m}$ is the velocity associated with parameter i for particle j at iteration m; ω_m is an inertial weight at iteration m; *rand* is a uniform random number $\in[0,1)$; $p_{i,j}$ is the current value of parameter i for particle j; $g\mathrm{best}_i$ is the value of parameter i attained at the global observed minimum; $p\mathrm{best}_{i,j}$ is the value of parameter i at the observed minimum for particle j; and $m_{\max}$ is the maximum number of iterations.

We employed a so-called absorbing boundary rule (Robinson & Rahmat-Samii, 2004), that is, if a parameter value would be displaced outside of the uncertainty interval (Table 1) during the displacement segment of the PSO, then the parameter value does not change and the particle velocity for that parameter is set to zero.

We obtained 375 accepted solutions ($\phi_{\mathrm{tot}} \leq -15$) of the PSO algorithm based on different random initial particle positions and velocities. Based on this, we then assess the sample frequency distribution of the identified model parameters conditional on the available information content (see Section 3). In this sense, our results correspond to a frequency analysis of a collection of model parameter estimates.

3. Results

We first present a collection of field observations and results from the calibrated model to facilitate grasping the main features of the system behavior. This provides a first quantitative appraisal of the type of observations and modeling results associated with the investigated complex system. This is followed by details of the GSA and the stochastic model calibration results.

3.1. Field-Scale Transport of Bacteria at the Stream-Groundwater Interface

3.1.1. Flow and Conservative Transport

Measured piezometric pressure head, temperature, and chloride concentrations are compared with the stochastic model calibration results obtained from the 375 PSO-based solutions at selected monitoring wells (Figure 2a—the complete set of calibration results are given in Figure S2 and S3). In general, PSO-based model solutions mimic the available data well. Uncertainty associated with the stochastic model calibration outputs is small for the target variables, that is, piezometric pressure head, temperature, and chloride concentration. For temperature, uncertainty increases between day 200 and 400, possibly due to the strong variability of river water temperature during this period. Differences between model calibration results and data are strongest for chloride due to the reduced sampling frequency and the higher measurement error (of the order of ~10% of the measured value), as compared to the one associated to piezometric pressure head and temperature data (~1%–2%).

The pattern of piezometric pressure heads indicates two flooding events around day 65 and day 435, respectively. Due to the high permeability of the gravel-sand aquifer, the hydraulic gradient between the river and observation well B is small, with values ranging between 0.5% (for small and intermediate river stage fluctuations) and 2% (for short times (<3 days) during large river stage changes, e.g., flooding events). Seasonal temperature fluctuations of the river can be observed at all vertical levels (B1, B2, and B3) with a delay in time of about 70 days (only data collected at B2 are included in Figure 2a). The highest measured groundwater temperature is 22°C at locations B3 and B2 (screens at 26 and 23 m a.s.l., respectively) and 20°C at B1 (19 m a.s.l.), these values being 5°C and 7°C below the maximum river temperature (27°C), respectively. Chloride concentrations in the river Rhine vary between 50 and 100 mg L^{-1}, denoting an increasing trend

during the simulation time. The time lag related to chloride signals in the river and observation points B1, B2, and B3 ranges between 20 and 30 days.

3.1.2. Reactive Transport of Oxygen and DOC/SOM Degradation

Due to organic carbon respiration, measured oxygen concentrations are generally lower in the aquifer than in the river (Figure 2a). Lowest values are observed between June and October (i.e., between days 200 and 350), when higher air and groundwater temperatures cause anoxic conditions at the observation wells. Furthermore, measured DOC remains constant at residual concentration, its value coinciding with non-reactive (not degradable) DOC components. Calibrated model results closely follow measured DOC values and capture the overall behavior of oxygen concentration, albeit a few details are not completely grasped by our model. For example, the reactive transport model does not properly show the oxygen maximum observed at day 150 at B2, the ensuing steep decrease until day 200, and the minimum displayed at day 400. Overall, measured oxygen concentrations are similar at well screens B1, B2, and B3, showing only a small variability between observation points (see Figure S3). For example, there is no oxygen maximum at day 150 at B1 and B3, and the increase of oxygen after the summer appeared slightly earlier at B1 (~day 350) than at B2 and B3 (~day 370). Observed differences between model results and data might be related to processes which are not included in the model, such as, for example, growth of microbes facilitating organic carbon respiration, complex organic carbon dynamics including SOC dissolution to DOC prior to oxidization and/or heterogeneous spatial distribution of microbes and SOC within the system.

3.1.3. Reactive Transport of Bacteria

Our model can mimic reasonably well measured concentrations of coliforms and *E. coli* (Figure 2b). However, measured patterns of bacteria concentrations are (overall) less accurately represented than conservative transport and organic carbon respiration (compare the quality of the results in Figure 2). This might be related to the observation that *E. coli* and coliform concentrations display a higher variability at differing depths (B3, B2, B1) than the physical-chemical variables (see Figures S2 and S3 with reference to temperature, chloride, and oxygen). An additional factor underlying these results might be attributed to the higher measurement error for microbiological laboratory analysis (20%–40%, Harmel et al. [2016]) compared to measurement errors for oxygen (≈5%), chloride (≈10%), and temperature (≈1%–2%).

Concentrations of coliforms are increasing above detection limit (i.e., 1 MPN/100 mL) during two periods (days 200–350, mostly TP III, and 435–450, TP V) (Figure 2b). The first period corresponds to the summer and is characterized by low river/groundwater levels, low groundwater flow velocities, high river/groundwater temperatures and low groundwater oxygen concentrations (Figure 2a). Enhanced bacteria transport can be related to the low oxygen concentrations, which slow down inactivation (Equation 8). *E. coli* bacteria were not detected in any of the observed wells during this period, concentrations of *E. coli* in the river being about 1–1.5 orders of magnitude lower than those of coliforms. Concentrations of the latter were observed to be 2 orders of magnitude above detection limit only once during this period. Thus, differences between *E. coli* and coliforms concentrations in the river (which are about 1–1.5 orders of magnitude) are a key factor for concentration differences of these species in groundwater (up to 2 orders of magnitude). Additionally, this concentration difference could indicate that inactivation of coliforms decreases stronger than that of *E. coli* due to the low oxygen concentrations in this period.

Both bacteria species are detected at all observation points in the second period (i.e., between days 435 and 450). This corresponds to a flooding event at the end of winter. Rising flow velocities and reduced residence times hamper the influence of inactivation and promote high bacteria concentrations. In contrast to the first period, high *E. coli* concentrations were also detected at the observation points. The key reason for higher *E. coli* concentration in groundwater is linked to an increased concentration in the river Rhine which might results from higher discharge of untreated wastewater into the river or changes in the wastewater treatment process during winter periods.

Concentrations of coliforms and *E. coli* during the flooding period were highest at B1 (with values of 201 and 41 MPN/100 mL, respectively) and lowest at B2 (4 and 1 MPN/100 mL). In contrast, highest concentrations of coliforms were observed during summer at well B2 (201 MPN/100 mL, based on 8 non-zero

measurements) and the lowest concentrations at B3 (19 MPN/100 mL, corresponding to the only non-zero measurement available). The documented difference between bacteria distribution during winter flood and summer might indicate (*i*) the effect of a subsurface heterogeneity which is somehow more complex than the one included in the model and allows for different transport pathways, depending on the flow regime and river stages, and/or (*ii*) some effects of biogeochemical heterogeneity, not included in the model. Biogeochemical heterogeneity was found in other studies to be a major element governing reaction rates (e.g., Boye et al. [2017]; Arora et al. [2016]). In our case, a heterogeneous distribution of heterogeneous distribution of iron oxides, could provide favorable attachment spots, or localized redox hotspots (as observed, e.g., by Briggs et al. (2018)) with low oxygen concentrations, could lead to locally decreased inactivation of bacteria.

The limited spatial resolution of the available data, especially along the direction perpendicular to the river, reduces our ability to account for subsurface heterogeneity in detail. Future studies with enhanced spatial resolution for data acquisition, perhaps in conjunction with modern hydrogeophysical methods, are needed to improve our ability to fully account for the subsurface heterogeneity. Additional benefits would also be gained by designing and implementing additional sampling of bacteria in closer proximity to the river to increase the amount of data associated with detection of bacteria and to be able to clearly distinguish the effects of the colmation layer and of the aquifer on bacteria retention.

Bacteria removal decreased from 4-log reduction (corresponding to a concentration reduction of 4 orders of magnitude) under optimal environmental conditions, which correspond to low (i.e., <1 m d^{-1}) groundwater flow velocities and oxic conditions, to a minimum of 2-log reduction under unfavorable conditions, these corresponding to anoxic conditions (occurring at the site at temperatures above 15°C) or groundwater flow velocities higher than 4 m d^{-1}. Bacteria removal per meter distance from the river ranged from 0.1-log reduction per m (optimal conditions) to 0.05-log reduction per m (unfavorable conditions). These removal rates are considered as low when compared to other field studies (Pang, 2009; Sprenger et al., 2014).

3.2. Global Sensitivity Analysis

Results from the sensitivity analysis enable one to quantify the influence of each parameter on target variables (Figure 3). As expected, parameter groups are only influential to target variables in case they are included into the corresponding process formulation. Values of Morris indices associated with model parameters show a significant variability over time and space, which is visible by the spread of the percentiles in Figure 3 (left). This result is also related to the temporal variability of boundary conditions (Section 3.3).

Figure 3 (right) depicts the ranking (based on the corresponding value of $\hat{\mu}^*_{j,k}$) of the importance of the various parameters with respect to each target variable. Note that the GSA suggests that k_{DOC} (parameter #24) and $K_{O2,DOC}$ (parameter #25) are the MSPs for the target variable DOC. However, in our data series, reactive DOC is always completely consumed at the observation points (Figures 2a and S3). Therefore, k_{DOC} and $K_{O2,DOC}$ would have little impact on model calibration as long as reactive DOC remains completely consumed. Then, these parameters (marked as exception in Figure 3) were not included in the set of MSP for stochastic model calibration. Additionally, the detachment coefficient for coliforms (parameter #32), which is slightly below the threshold we set for the identification of MSP (Equation 15), was included within MSP to retain the same set of species-specific parameters for coliforms and *E. coli*.

Overall, 26 of the 59 uncertain parameters detailed in Table 1 are retained for the stochastic model calibration. The parameters in MSP *are* marked with "*" in Table 1 and identified with colors in Figure 3 (right).

3.2.1. Flow and Conservative Transport

Parameters employed to evaluate permeability (i.e., porosity and specific surface area, corresponding to parameters #15–16, and #1–2, respectively, for both aquifer zones; and parameters #3–7 for the colmation layer; see Table 1) and grouped as *permeability parameters* are sensitive to simulated piezometric pressure heads. Permeability parameters of the lower aquifer (i.e., parameters #1 and #15) display a higher sensitiv-

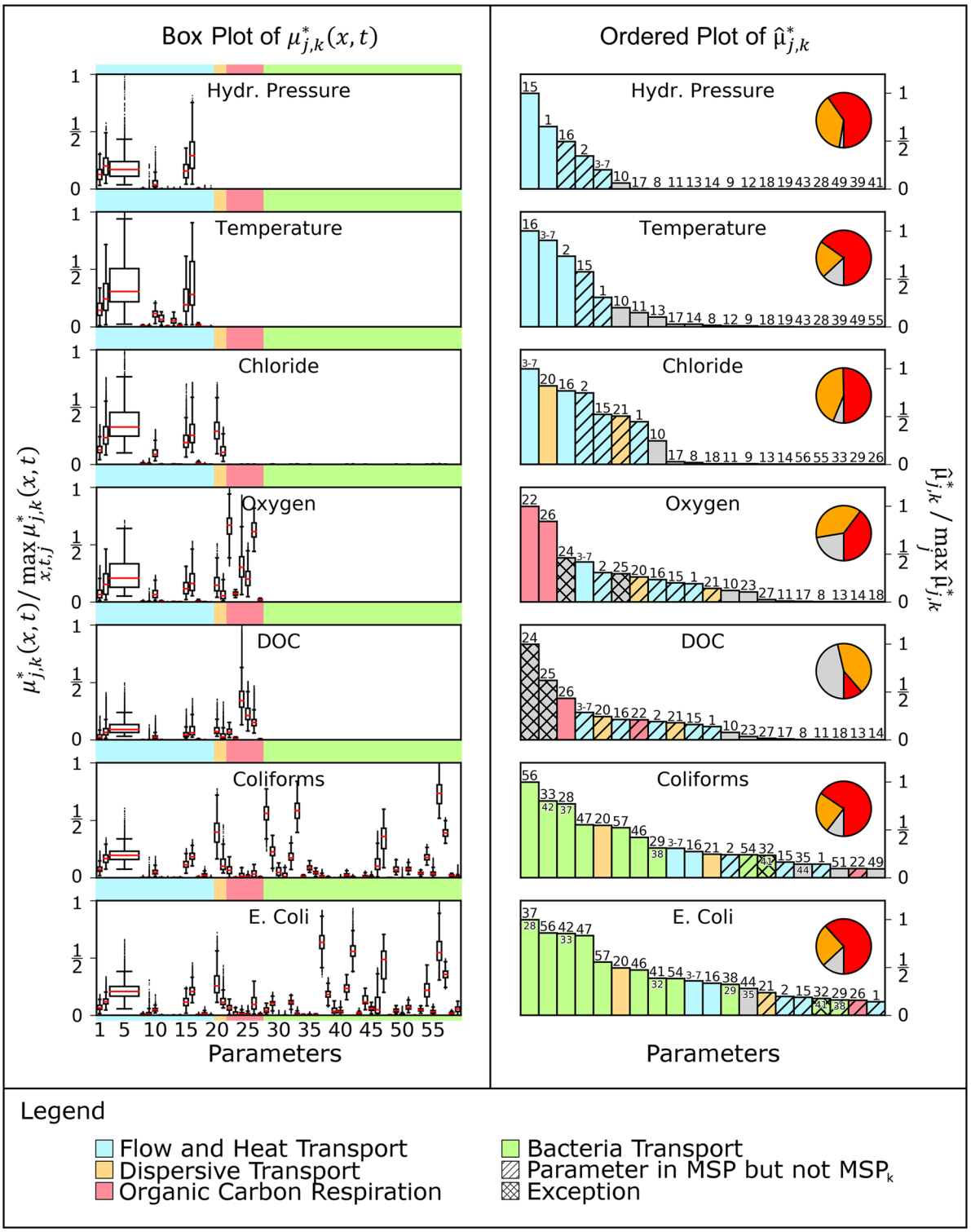

Figure 3. Left: Box plot of $\mu^*_{j,k}(x,t)$ for each target variable for all parameters across all timesteps and observation points; each parameter group is denoted by a given color code. Parameters #{3–7} are grouped on the basis of Equation 14, the ensuing result being depicted as a wider box for ease of visualization. Right: Ordered bar plot of values of $\hat{\mu}^*_{j,k}$ for all target variables, showing only the 20 parameters associated with the highest rank. Parameters included in the set MSP are identified by colors. The number above each column corresponds to the parameter number (see Table 1). Numbers below these identify the corresponding species-specific parameter of the second bacteria (e.g., particle size for coliforms (#33) and for *E. coli* (#42)). The figure includes pie diagrams showing MSP_k (red color, $\sum_{j \in MSP_k} \hat{\mu}^*_{j,k}$) and MSP (red + orange colors, $\sum_{j \in MSP} \hat{\mu}^*_{j,k}$) as a fraction of $\sum_j \hat{\mu}^*_{j,k}$ (depicted through red + orange + gray colors) for each output variable k. Exceptions to the MSP criteria in Equation 15 are described in the main text.

ity than those of the upper aquifer and colmation layer. This is related to the observation that the GSA for piezometric pressure heads only targeted the lower aquifer (Equation 13), since data were only available at B1. Sensitivity of porosity is higher than that of the specific surface area for both aquifer layers.

Permeability parameters are markedly sensitive also for the simulation of heat transport. Colmation layer permeability is more sensitive than the permeability parameters of the aquifer layers because of the governing role of the colmation layer on inflow to the riverbank. A low colmation layer permeability results in flow being directed more through the riverbed (Zone 5) than through the riverbank (Zone 6). Sensitivity to temperature of the permeability parameters of the upper aquifer is higher than that of their counterparts associated with the lower aquifer because B3 is more directly influenced by temperature changes in the river. The influence of thermal parameters (i.e., parameters #11–14) is relatively modest as the parameter variability range for gravel sand sediments is fairly limited.

Sensitivity of the colmation layer permeability (parameter #3–7) to chloride transport is the highest one. This indicates an increased influence of the colmation layer (and with it the inflow through riverbed or riverbank) on chloride as compared to temperature. Longitudinal dispersivity (parameter #20) is the second MSP, dispersive transport being only slightly less significant than advective transport at the stream-groundwater interface.

3.2.2. Reactive and Bacteria Transport

Organic carbon respiration parameters are the most sensitive to reactive transport of oxygen and DOC. The rate constant for SOC (parameter #22) is more sensitive to oxygen than the rate constant for DOC (#24), possibly resulting from the limited inflow of reactive DOC from the river. Sensitivity of parameter β (#26) is also markedly notable, suggesting the strong impact of temperature on reaction rates. With reference to the dispersive and advective transport parameters, their order in the sensitivity ranking is similar to what was observed for chloride.

The MSPs to bacteria transport (here identified through the dynamics of coliforms (CF) and *E. coli* (EC)) are the coefficients associated with inactivation and straining and corresponding to the inactivation coefficients for the mobile phase (parameter #28, ranked third for CF in Figure 3 (right); parameter #37, first for EC), the straining coefficients (#56, first for CF and second for EC), and exponent (#57, sixth for CF and fifth for EC) and inactivation coefficients in the immobile phase (#29, eighth for CF; #38, 12th for EC).

With the exception of particle size of both bacteria (#33, second for CF; #42, third for EC) and sediments (#47, fourth for CF and fourth for EC), all parameters related to DLVO calculations display a minimal sensitivity across the selected range of variability. The most sensitive one within this subgroup was the Hamaker Coefficient (#35, 16th for CF; #44, 13th for EC). We note that this result does not exclude the possibility of a strong nonlinear influence of the latter parameter or that there are joint effects on model outcomes by multiple parameters used in the DLVO calculations. This feature cannot be disentangled by the analyses of the Morris indices (Equation 12) and can be worth of a targeted future investigation.

Detachment coefficients (#32, 14th for CF; #41, eighth for EC) and the maximum immobile bacteria concentration in the aquifer (#54, 13th for CF and ninth for EC) are characterized by a medium sensitivity. Therefore, parameters driving the elimination processes (i.e., inactivation and straining) have a higher impact on modeling results than those associated with attachment/detachment. However, this is not completely distinguishable, as both bacteria and grain size are highly relevant for straining and attachment.

Sensitivity of parameters linked to the feedback between oxygen concentration and inactivation (#30, 31, 39, 40, 59) is visibly low. The MSP of this group is the inactivation coefficient ratio (parameter #30) and is only ranked as 26th. The oxidation rate constant for SOC (#22, 19th for CF) and the β parameter (#26, 19th for EC) are more sensitive than the inactivation coefficient ratio, their relevance being still ranked as low. As such, one can conclude that the dependency of inactivation on the oxygen concentration has only a limited impact on bacteria concentrations. For a change of the parameter value of the anoxic to oxic inactivation coefficient ratios (parameters #30, 31, 39, 40) to significantly impact bacteria concentrations, two conditions need to take place: (*i*) oxygen concentrations are below the threshold value and (*ii*) the values of the inac-

tivation coefficients under oxic conditions are sufficiently high. Since the Morris indices are based on the mean of a set of EEs evaluated across the parameter space (Equation 12) and the two conditions will only apply in a subregion of the overall parameter space, the value of the EEs for this parameter will be near zero outside of such a subregion, thus resulting in a low Morris index value.

This can be illustrated by considering as an example the EEs associated with the output variable coliform concentration at location B1 along well B. In this case, the highest values of the EEs associated with parameters linked to the feedback between oxygen concentration and inactivation (#22, 30) are about 15% lower than the corresponding values related to the EEs linked to dispersivity (#20) or to the inactivation coefficient under oxic conditions (#28). Furthermore, the distributions of the EEs related to parameters #22 and 30 are much more skewed (with more than 90% of the EEs being near zero) compared to those for parameters #20 and 28 (50% and 40% of the EEs are near zero), as also seen in Figure S4 of the supporting information. This result suggests that, while parameters related to the feedback between oxygen concentrations and inactivation (e.g., #22 and 30) can have a significant effect on coliform concentrations, their influence is relevant only within a small subregion of the parameter space. The Morris index (i.e., the mean of the EEs evaluated across the entire parameter space) can therefore underestimate the sensitivity of a parameter if the parameter is only relevant under specific conditions (as, e.g., for inactivation coefficient ratios for anoxic conditions) as compared to parameters which are relevant across the entire parameter space, for example, permeability. We note that reliance on Morris indices to evaluate the relative importance of model parameters enables one to extend the results to the whole parameter space in case the behavior of the model is linear with respect to input parameters. A clear demarcation of the detailed model behavior within subregions of the parameter space can be obtained, for example, though the approach based on the distributed evaluation of local sensitivity analysis (DELSA; Rakovec et al., 2014; Ceriotti et al., 2018 and references therein). The latter is based on a set of evaluations of a local sensitivity metric across a (typically regular) grid in the parameter space. It is well recognized that an aspect limiting the application of the DELSA approach is the potentially large amount of sensitivity maps that one can obtain. The latter aspect is markedly challenging in scenarios of the kind we investigate, involving a considerably high number of parameters and temporal intervals of interest. In this context, the effective implementation of this approach will be subject to future investigations, eventually in conjunction with formulation of surrogate modeling strategies to alleviate computational burden and advanced data analysis techniques to extract relevant patterns from the amount of information generated by model simulations.

3.3. Impact of Hydrological Events on Temporal Dynamics of Parameter Sensitivity

A correspondence between river level fluctuations and the ensuing value of the Morris index associated with some parameters (e.g., inactivation coefficient for coliforms and longitudinal dispersivity) can be observed (Figure 4). For example, a quick increase of the river level (as noted at day 330 and 430) is related to a decrease of the Morris index associated with the inactivation coefficient, corresponding to a decreased sensitivity of inactivation to bacteria concentration. This is consistent with the enhanced flow velocities due to the rapid increase of the river level (and of the hydraulic gradient). Indeed, an increased flow velocity leads to reduced travel times for bacteria toward the observation wells and, in turn, to a reduced temporal window within which inactivation can eventually take place. Therefore, a change in the inactivation coefficient will have less impact on bacteria concentrations for high flow velocities, as compared to periods characterized by longer travel times. Otherwise, the impact of dispersivity increases with the river stage (and the groundwater pressure head gradient), because high flow velocities correspond to an increased dispersion coefficient. In general, we can observe that the variations of boundary conditions, for example of seasonal origin, can influence the relative importance of different transport processes. However, we note that other effects can affect the temporal variability of the sensitivity of a parameter. For example, gradually filling up of the limited attachment spots for bacteria on the sediment could lead to a lower sensitivity for attachment related parameters. While we observed such correspondences, a complete characterization of these aiming for more general conclusions is out of the scope of this work.

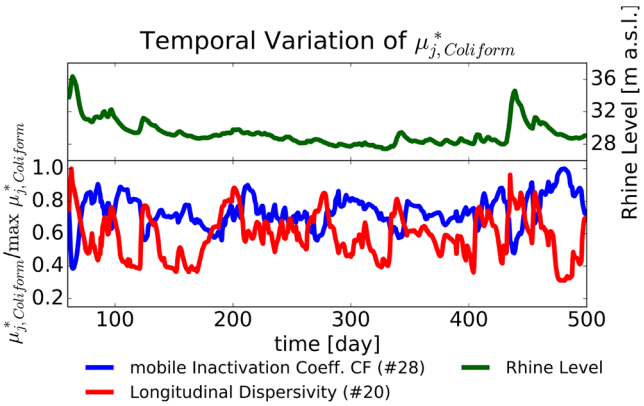

Figure 4. Temporal variation of $\mu^*_{j,k}(\boldsymbol{x},t)$ evaluated for coliform concentration at observation point B2 for two selected parameters (inactivation coefficient for mobile coliforms under oxic conditions and longitudinal dispersivity).

3.4. Stochastic Calibration Results

Histograms of parameter values obtained from the collection of the 375 inverse modeling runs are depicted in Figure 5. Overall, we can observe that conditioning on data has a beneficial effect in reducing the uncertainty associated with hydraulic and organic carbon respiration parameters, while it does not impact significantly the prior uncertainty linked to parameters for dispersive transport and those specific to bacteria transport.

Estimated porosities for the aquifer layers (parameters #15 and #16) tend to be concentrated around high values within the selected parameter range (with mode displayed at values of 0.385 and 0.295, respectively). The opposite behavior is documented for the specific surface area per unit volume (#1 and #2; mode at 6602 and 8161 m^{-1}, respectively). These results are consistent with high permeability values in the aquifer layers, as driven by Equation 1. This behavior is enhanced for the lower aquifer (layer Z2; parameters #1 and #15), indicating a higher permeability of this layer as compared to the upper aquifer. With reference to the colmation layer permeability, period I, II, and IV tend to be associated with the highest values (mode of permeability values equal to 2.5×10^{-11} m^2, 6.3×10^{-11} m^2, and 2.5×10^{-11} m^2 for periods I, II, and IV, respectively), low values being observed across time periods III and V (with mode equal to 2.5×10^{-13} m^2 and 4.0×10^{-14} m^2 for periods III and V, respectively). This would indicate an increased clogging during summer (period III) due to enhanced biogeochemical activity (bio-clogging). Period I and V correspond to flooding events at the end of the winter. It can be assumed that their characteristics (in terms of, e.g., sediment load) are similar. However, they show different trends in their corresponding parameter value histograms, a behavior which might be related to data availability, as there was a more detailed sampling for bacteria during period V.

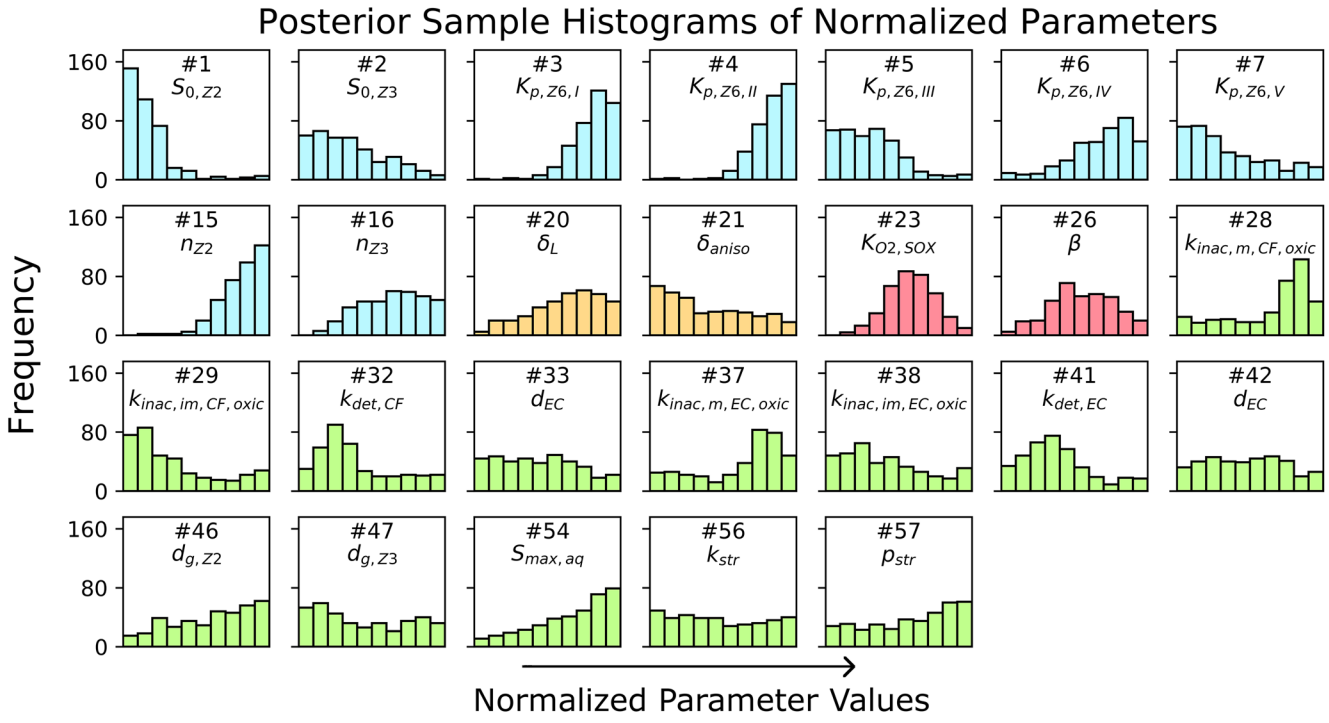

Figure 5. Histograms of parameter values obtained from the collection of inverse modeling results. Parameter values are normalized within the interval [0,1] associated with the range of variability considered (Table 1). Colors highlight parameter groups (see Table 1 and Figure 3).

While longitudinal dispersivity (parameter #20), straining coefficients (#56, 57), and bacteria size (#33, 42) are among the MSPs (Figure 3), their posterior distributions are close to the prior (uniform) distribution. This result suggests that the available data are not highly informative to constrain their value, as embedded in the mathematical formulation employed. Otherwise, the inactivation coefficients (#28, 29, 37, 38) and the detachment coefficients (#32, 41) are all characterized by a clearly identifiable peak in their posterior distribution. Inactivation coefficients for the mobile phase (#28, 37) are characterized by values (mode at 1.4×10 and 6.0×10^{-1} d^{-1}, respectively) which are significantly larger than those associated with the immobile phase (#29, 38, with mode at 3.6×10^{-3} and 8.4×10^{-3} d^{-1}, respectively).

Detachment coefficients (#32, 41) also display low values (mode at 4.7×10^{-3} and 2.2×10^{-2} d^{-1}) as compared to inactivation (e.g., mode of #28 at 1.4 d^{-1}), suggesting that remobilization of attached bacteria occurs at a slower pace. Overall, parameters associated with coliform transport show a higher reduction in uncertainty due to conditioning on the available data as compared to parameters linked to *E. coli* transport. This result is possibly related to the higher number of non-zero measurements available for coliforms than for *E. coli* (Figure 2b and Equation 16).

4. Conclusions

Our work leads to the following main conclusions.

1. Based on the GSA performed, model parameters characterizing bacteria elimination processes (i.e., inactivation and straining) are key for bacteria transport at the riverbank filtration site analyzed. This finding can have important consequences on the level of uncertainty associated with modeling results because inactivation and straining coefficients are influenced by a variety of factors (e.g., presence of other biota, geometrical features of the pore space) and are therefore very difficult to determine for field conditions. The high sensitivity of the bacteria size suggests that bacteria with differing size can be characterized by significantly different transport behavior. This, in turn, highlights that considering a single pathogen species, that is, *E. coli*, in a modeling study is not conducive to an accurate assessment of the risk for contamination related to other pathogen species.
2. Permeability of the colmation layer at the site is also influential to control bacteria transport to groundwater. Seasonal changes of permeability due to bio-clogging in summer and reduction of low-permeability riverbed sediments during winter floods can lead to significant changes in bacteria residence times. These can in turn give rise to longer or shorter transport paths, thus impacting the risk for bacteria contamination of drinking water wells. Temporal variability of the colmation layer permeability is not trivial to monitor over the years and can therefore induce significant uncertainty to predictions of field-scale bacteria transport.
3. Data from a 1-year monitoring campaign and modeling results suggest that bacteria transport is markedly driven by seasonal variations of the river stage, temperature, and oxygen content. As GSA indicates, this result can be mainly attributed to changes associated with inactivation. The summer period (with anoxic aquifer conditions) and the flooding event at the end of winter season (with increased flow velocities) are both associated with high bacteria concentrations in groundwater. Anoxic aquifer conditions (in the summer period) as well as increased groundwater flow velocities and associated reduced residence times (during the winter flood) lead to a reduced impact of inactivation.
4. Even as the available data set is quite detailed, results from our stochastic inverse modeling analysis suggest that collected measurements are not entirely effective in constraining uncertainty associated with some model parameters (e.g., longitudinal dispersivity, straining coefficients, and bacteria size) for coliform and *E. coli* transport. Otherwise, conditioning on available data enables one to constrain uncertainty associated with the inactivation and the detachment coefficients.

As described in Section 2.4, our GSA is placed before model calibration and relies on the working hypothesis that model parameters are uncorrelated. This assumption is employed due to the lack of information about firm quantifiable degrees of correlation among the 59 model parameters embedded in the model. In cases where it is possible to quantify such correlations, the GSA could then be performed upon sampling from the ensuing joint distribution of model parameters (see e.g., Dell'Oca et al., 2020 and references therein). This could impact the ranking of model parameters, an element which deserves future investigations to further enhance our understanding of the functioning of the interpretive model and system considered.

Another element deserving future detailed developments is related to the identification of parameters having the largest impact on the residual uncertainty of model output, that is, the uncertainty still remaining after model calibration. In this context, the GSA would be constrained to model calibration and could be employed to guiding additional efforts for parameter characterization. The probability density function associated with each model parameter at this stage is typically different from the one considered prior to model calibration and might include cross-correlations amongst model parameters (see, e.g., Dell'Oca et al., 2020 and references therein for additional details on this).

In summary, from a waterworks management perspective, the high uncertainty still affecting simulation of bacteria transport is still recognized as a remarkable challenge. While model parameters can be very influential, as shown in our study, they can be very hard to assess at field scale. The highest contributions to the uncertainty associated with bacteria transport results stem from inactivation coefficients (1), the time-variant colmation layer permeability (2), as well as seasonal effects such as floods and changes of oxic to anoxic conditions (3). While (2) and (3) could be better estimated by proxies, such as temperature, oxygen content, or Eh values (1) is markedly difficult to quantify even at laboratory scale for field conditions and can only be assessed by considering it as a model calibration parameter at the field scale. In this context, our study underpins the need for improved understanding of these reactive transport processes and parameter relevance to increase the predictive accuracy of model results which can later the used as basis for a risk-based management decisions process for waterworks using bank filtration for drinking water production.

Data Availability Statement

Supporting information and data for this research are available at http://dx.doi.org/10.14279/depositonce-10014.

Conflict of Interest

The authors declare no conflicts of interest relevant to this study.

Acknowledgments
We would like to thank the Deutsche Bundesstiftung Umwelt (DBU) for funding (D. Knabe). Furthermore, we would like to thank the North-German Supercomputing Alliance (HLRN) for supercomputing resources. We gratefully acknowledge the Stadtwerke Düsseldorf for providing the data and further information about the site. Additionally, we thank Aronne dell'Oca for providing Matlab scripts as basis for the Morris Index calculations and the PSO algorithm.

References

Argent, J., Torkzaban, S., Hubbard, S., Le, H., Amirianshoja, T., & Haghighi, M. (2015). Visualization of micro-particle retention on a heterogeneous surface using micro-models: Influence of nanoscale surface roughness. *Transport in Porous Media*, *109*(2), 239–253. https://doi.org/10.1007/s11242-015-0511-z

Arora, B., Spycher, N. F., Steefel, C. I., Molins, S., Bill, M., Conrad, M. E., et al. (2016). Influence of hydrological, biogeochemical and temperature transients on subsurface carbon fluxes in a flood plain environment. *Biogeochemistry*, *127*(2), 367–396. https://doi.org/10.1007/s10533-016-0186-8

Bayer, P., Comunian, A., Höyng, D., & Mariethoz, G. (2015). High resolution multi-facies realizations of sedimentary reservoir and aquifer analogs. *Scientific Data*, *2*(1), 150033. https://doi.org/10.1038/sdata.2015.33

Bianchi Janetti, E., Guadagnini, L., Riva, M., & Guadagnini, A. (2019). Global sensitivity analyses of multiple conceptual models with uncertain parameters driving groundwater flow in a regional-scale sedimentary aquifer. *Journal of Hydrology*, *574*, 544–556. https://doi.org/10.1016/j.jhydrol.2019.04.035

Blaschke, A. P., Derx, J., Zessner, M., Kirnbauer, R., Kavka, G., Strelec, H., et al. (2016). Setback distances between small biological wastewater treatment systems and drinking water wells against virus contamination in alluvial aquifers. *Science of The Total Environment*, *573*, 278–289. https://doi.org/10.1016/j.scitotenv.2016.08.075

Blaustein, R. A., Pachepsky, Y., Hill, R. L., Shelton, D. R., & Whelan, G. (2013). *Escherichia coli* survival in waters: Temperature dependence. *Water Research*, *47*(2), 569–578. https://doi.org/10.1016/j.watres.2012.10.027

Boye, K., Noël, V., Tfaily, M. M., Bone, S. E., Williams, K. H., Bargar, J. R., & Fendorf, S. (2017). Thermodynamically controlled preservation of organic carbon in floodplains. *Nature Geoscience*, *10*(6), 415–419. https://doi.org/10.1038/ngeo2940

Bradford, S. A., Simunek, J., Bettahar, M., van Genuchten, M. T., & Yates, S. R. (2003). Modeling colloid attachment, straining, and exclusion in saturated porous media. *Environmental Science & Technology*, *37*(10), 2242–2250. https://doi.org/10.1021/es025899u

Bradford, S. A., Torkzaban, S., Leij, F., & Simunek, J. (2015). Equilibrium and kinetic models for colloid release under transient solution chemistry conditions. *Journal of Contaminant Hydrology*, *181*, 141–152. https://doi.org/10.1016/j.jconhyd.2015.04.003

Briggs, M. A., Day-Lewis, F. D., Dehkordy, F. M. P., Hampton, T., Zarnetske, J. P., Scruggs, C. R., et al. (2018). Direct observations of hydrologic exchange occurring with less-mobile porosity and the development of anoxic microzones in sandy lakebed sediments. *Water Resources Research*, *54*(7), 4714–4729. https://doi.org/10.1029/2018wr022823

Brown, D. G., & Jaffé, P. R. (2006). Effects of nonionic surfactants on the cell surface hydrophobicity and apparent Hamaker constant of a *Sphingomonas* sp. *Environmental Science & Technology*, *40*(1), 195–201. https://doi.org/10.1021/es051183y

Campolongo, F., Cariboni, J., & Saltelli, A. (2007). An effective screening design for sensitivity analysis of large models. *Environmental Modelling & Software*, *22*(10), 1509–1518. https://doi.org/10.1016/j.envsoft.2006.10.004

Carrier, W. D. (2003). Goodbye, Hazen; Hello, Kozeny-Carman. *Journal of Geotechnical & Geoenvironmental Engineering*, *129*(11), 1054–1056. https://doi.org/10.1061/(asce)1090-0241(2003)129:11(1054)

Castagna, M., & Bellin, A. (2009). A Bayesian approach for inversion of hydraulic tomographic data. *Water Resources Research*, *45*, W04410. https://doi.org/10.1029/2008wr007078

Ceriotti, G., Guadagnini, L., Porta, G., & Guadagnini, A. (2018). Local and global sensitivity analysis of Cr (VI) geogenic leakage under uncertain environmental conditions. *Water Resources Research*, *54*, 5785–5802. https://doi.org/10.1029/2018wr022857

Chen, G., & Walker, S. L. (2007). Role of solution chemistry and ion valence on the adhesion kinetics of groundwater and marine bacteria. *Langmuir*, *23*(13), 7162–7169. https://doi.org/10.1021/la0632833

Chrysikopoulos, C. V., & Aravantinou, A. F. (2014). Virus attachment onto quartz sand: Role of grain size and temperature. *Journal of Environmental Chemical Engineering*, *2*(2), 796–801. https://doi.org/10.1016/j.jece.2014.01.025

Chu, Y., Jin, Y., Baumann, T., & Yates, M. V. (2003). Effect of soil properties on saturated and unsaturated virus transport through columns. *Journal of Environmental Quality*, *32*(6), 2017–2025. https://doi.org/10.2134/jeq2003.2017

Ciriello, V., Guadagnini, A., Di Federico, V., Edery, Y., & Berkowitz, B. (2013). Comparative analysis of formulations for conservative transport in porous media through sensitivity-based parameter calibration. *Water Resources Research*, *49*(9), 5206–5220. https://doi.org/10.1002/wrcr.20395

Council Directive 98/83/EC of 3 November 1998. (1998). On the quality of water intended for human consumption. *Official Journal*, *L330*, 32–54.

Dell'Oca, A., Riva, M., & Guadagnini, A. (2020). Global sensitivity analysis for multiple interpretive models with uncertain parameters. *Water Resources Research*, *56*(2), e25754. https://doi.org/10.1029/2019WR025754

de Roda Husman, A. M., Lodder, W. J., Rutjes, S. A., Schijven, J. F., & Teunis, P. F. M. (2009). Long-term inactivation study of three enteroviruses in artificial surface and groundwaters, using PCR and cell culture. *Applied and Environmental Microbiology*, *75*(4), 1050. https://doi.org/10.1128/aem.01750-08

Derx, J., Blaschke, A. P., Farnleitner, A. H., Pang, L., Blöschl, G., & Schijven, J. F. (2013). Effects of fluctuations in river water level on virus removal by bank filtration and aquifer passage – A scenario analysis. *Journal of Contaminant Hydrology*, *147*, 34–44. https://doi.org/10.1016/j.jconhyd.2013.01.001

Dwivedi, D., Steefel, C. I., Arora, B., Newcomer, M., Moulton, J. D., Dafflon, B., et al. (2018). Geochemical exports to river from the intrameander hyporheic zone under transient hydrologic conditions: East River Mountainous Watershed, Colorado. *Water Resources Research*, *54*(10), 8456–8477. https://doi.org/10.1029/2018wr023377

Feighery, J., Mailloux, B. J., Ferguson, A. S., Ahmed, K. M., van Geen, A., & Culligan, P. J. (2013). Transport of *E. coli* in aquifer sediments of Bangladesh: Implications for widespread microbial contamination of groundwater. *Water Resources Research*, *49*(7), 3897–3911. https://doi.org/10.1002/wrcr.20289

Feke, D. L., Prabhu, N. D., Mann, J. A., & Mann, J. A. (1984). A formulation of the short-range repulsion between spherical colloidal particles. *The Journal of Physical Chemistry A*, *88*(23), 5735–5739. https://doi.org/10.1021/j150667a055

Foppen, J. W. A., van Herwerden, M., Kebtie, M., Noman, A., Schijven, J. F., Stuyfzand, P. J., & Uhlenbrook, S. (2008). Transport of *Escherichia coli* and solutes during waste water infiltration in an urban alluvial aquifer. *Journal of Contaminant Hydrology*, *95*(1), 1–16. https://doi.org/10.1016/j.jconhyd.2007.07.005

Gerardi, M. H., & Zimmerman, M. C. (2005). Bacteria. In M. H. Gerardi (Ed.), *Wastewater pathogens* (pp. 53–66). John Wiley & Sons, Ltd. https://doi.org/10.1002/0471710431.ch9

Gillefalk, M., Massmann, G., Nützmann, G., & Hilt, S. (2018). Potential impacts of induced bank filtration on surface water quality: A conceptual framework for future research. *Water*, *10*(9), 1240. https://doi.org/10.3390/w10091240

Gordon, C., & Toze, S. (2003). Influence of groundwater characteristics on the survival of enteric viruses. *Journal of Applied Microbiology*, *95*(3), 536–544. https://doi.org/10.1046/j.1365-2672.2003.02010.x

Gregory, J. (1981). Approximate expressions for retarded van der waals interaction. *Journal of Colloid and Interface Science*, *83*(1), 138–145. https://doi.org/10.1016/0021-9797(81)90018-7

Harmel, R. D., Hathaway, J. M., Wagner, K. L., Wolfe, J. E., Karthikeyan, R., Francesconi, W., & McCarthy, D. T. (2016). Uncertainty in monitoring *E. coli* concentrations in streams and stormwater runoff. *Journal of Hydrology*, *534*, 524–533. https://doi.org/10.1016/j.jhydrol.2016.01.040

Hatch, C. E., Fisher, A. T., Ruehl, C. R., & Stemler, G. (2010). Spatial and temporal variations in streambed hydraulic conductivity quantified with time-series thermal methods. *Journal of Hydrology*, *389*(3), 276–288. https://doi.org/10.1016/j.jhydrol.2010.05.046

Hilpert, M., & Johnson, W. P. (2018). A binomial modeling approach for upscaling colloid transport under unfavorable attachment conditions: Emergent prediction of nonmonotonic retention profiles. *Water Resources Research*, *54*(1), 46–60. https://doi.org/10.1002/2017wr021454

Hogg, R., Healy, T. W., & Fuerstenau, D. W. (1966). Mutual coagulation of colloidal dispersions. *Transactions of the Faraday Society*, *62*, 1638–1651. https://doi.org/10.1039/tf9666201638

Hornstra, L. M., Schijven, J. F., Waade, A., Prat, G. S., Smits, F. J. C., Cirkel, G., et al. (2018). Transport of bacteriophage MS2 and PRD1 in saturated dune sand under suboxic conditions. *Water Research*, *139*, 158–167. https://doi.org/10.1016/j.watres.2018.03.054

Hunt, R. J., & Johnson, W. P. (2017). Pathogen transport in groundwater systems: Contrasts with traditional solute transport. *Hydrogeology Journal*, *25*(4), 921–930. https://doi.org/10.1007/s10040-016-1502-z

Johnson, W. P., Rasmuson, A., Pazmiño, E., & Hilpert, M. (2018). Why variant colloid transport behaviors emerge among identical individuals in porous media when colloid-surface repulsion exists. *Environmental Science & Technology*, *52*(13), 7230–7239. https://doi.org/10.1021/acs.est.8b00811

Johnson, W. P., Tong, M., & Li, X. (2007). On colloid retention in saturated porous media in the presence of energy barriers: The failure of α, and opportunities to predict η. *Water Resources Research*, *43*, W12S13. https://doi.org/10.1029/2006wr005770

Kvitsand, H. M. L., Ilyas, A., & Østerhus, S. W. (2015). Rapid bacteriophage MS2 transport in an oxic sandy aquifer in cold climate: Field experiments and modeling. *Water Resources Research*, *51*(12), 9725–9745. https://doi.org/10.1002/2015wr017863

Laloy, E., Rogiers, B., Vrugt, J. A., Mallants, D., & Jacques, D. (2013). Efficient posterior exploration of a high-dimensional groundwater model from two-stage Markov chain Monte Carlo simulation and polynomial chaos expansion. *Water Resources Research*, *49*(5), 2664–2682. https://doi.org/10.1002/wrcr.20226

Levy, J., Sun, K., Findlay, R. H., Farruggia, F. T., Porter, J., Mumy, K. L., et al. (2007). Transport of *Escherichia coli* bacteria through laboratory columns of glacial-outwash sediments: Estimating model parameter values based on sediment characteristics. *Journal of Contaminant Hydrology*, *89*(1), 71–106. https://doi.org/10.1016/j.jconhyd.2006.08.006

Lewis, C. L., Craig, C. C., & Senecal, A. G. (2014). Mass and density measurements of live and dead Gram-negative and Gram-positive bacterial populations. *Applied and Environmental Microbiology*, *80*(12), 3622–3631. https://doi.org/10.1128/aem.00117-14

Lichtner, P. C., Hammond, G. E., Lu, C., Karra, S., Bisht, G., Andre, B., et al. (2019). *PFLOTRAN user manual*. Retrieved from http://documentation.pflotran.org

Li, J., Zhao, X., Tian, X., Li, J., Sjollema, J., & Wang, A. (2015). Retention in treated wastewater affects survival and deposition of *Staphylococcus aureus* and *Escherichia coli* in sand columns. *Applied and Environmental Microbiology*, *81*(6), 2199–2205. https://doi.org/10.1128/aem.03740-14

Majone, B., Bovolo, C. I., Bellin, A., Blenkinsop, S., & Fowler, H. J. (2012). Modeling the impacts of future climate change on water resources for the Gállego river basin (Spain). *Water Resources Research*, *48*, W01512. https://doi.org/10.1029/2011wr010985

Mayotte, J.-M., Hölting, L., & Bishop, K. (2017). Reduced removal of bacteriophage MS2 in during basin infiltration managed aquifer recharge as basin sand is exposed to infiltration water. *Hydrological Processes*, *31*(9), 1690–1701. https://doi.org/10.1002/hyp.11137

Messina, F., Marchisio, D. L., & Sethi, R. (2015). An extended and total flux normalized correlation equation for predicting single-collector efficiency. *Journal of Colloid and Interface Science*, *446*, 185–193. https://doi.org/10.1016/j.jcis.2015.01.024

Molnar, I. L., Johnson, W. P., Gerhard, J. I., Willson, C. S., & O'Carroll, D. M. (2015). Predicting colloid transport through saturated porous media: A critical review. *Water Resources Research*, *51*(9), 6804–6845. https://doi.org/10.1002/2015wr017318

Mondal, P. K., & Sleep, B. E. (2013). Virus and virus-sized microsphere transport in a dolomite rock fracture. *Water Resources Research*, *49*(2), 808–824. https://doi.org/10.1002/wrcr.20086

Morris, M. D. (1991). Factorial sampling plans for preliminary computational experiments. *Technometrics*, *33*(2), 161–174. https://doi.org/10.1080/00401706.1991.10484804

Pang, L. (2009). Microbial removal rates in subsurface media estimated from published studies of field experiments and large intact soil cores. *Journal of Environmental Quality*, *38*(4), 1531–1559. https://doi.org/10.2134/jeq2008.0379

Park, J.-A., Kang, J.-K., & Kim, S.-B. (2017). Comparative analysis of bacteriophages and bacteria removal in soils and pyrophyllite-amended soils: Column experiments. *Water, Air, & Soil Pollution*, *228*(3), 103. https://doi.org/10.1007/s11270-017-3288-6

Porta, G., La Cecilia, D., Guadagnini, A., & Maggi, F. (2018). Implications of uncertain bioreactive parameters on a complex reaction network of atrazine biodegradation in soil. *Advances in Water Resources*, *121*, 263–276. https://doi.org/10.1016/j.advwatres.2018.08.002

Rakovec, O., Hill, M. C., Clark, M. P., Weerts, A. H., Teuling, A. J., & Uijlenhoet, R. (2014). Distributed evaluation of local sensitivity analysis (DELSA), with application to hydrologic models. *Water Resources Research*, *50*(1), 409–426. https://doi.org/10.1002/2013wr014063

Redman, J. A., Walker, S. L., & Elimelech, M. (2004). Bacterial adhesion and transport in porous media: Role of the secondary energy minimum. *Environmental Science & Technology*, *38*(6), 1777–1785. https://doi.org/10.1021/es034887l

Robinson, J., & Rahmat-Samii, Y. (2004). Particle swarm optimization in electromagnetics. *IEEE Transactions on Antennas and Propagation*, *52*(2), 397–407. https://doi.org/10.1109/tap.2004.823969

Russian, A., Riva, M., Russo, E. R., Chiaramonte, M. A., & Guadagnini, A. (2019). Stochastic inverse modeling and global sensitivity analysis to assist interpretation of drilling mud losses in fractured formations. *Stochastic Environmental Research and Risk Assessment*, *33*(10), 1681–1697. https://doi.org/10.1007/s00477-019-01729-4

Sadeghi, G., Behrends, T., Schijven, J. F., & Hassanizadeh, S. M. (2013). Effect of dissolved calcium on the removal of bacteriophage PRD1 during soil passage: The role of double-layer interactions. *Journal of Contaminant Hydrology*, *144*(1), 78–87. https://doi.org/10.1016/j.jconhyd.2012.10.006

Sasidharan, S., Torkzaban, S., Bradford, S. A., Cook, P. G., & Gupta, V. V. S. R. (2017). Temperature dependency of virus and nanoparticle transport and retention in saturated porous media. *Journal of Contaminant Hydrology*, *196*, 10–20. https://doi.org/10.1016/j.jconhyd.2016.11.004

Schijven, J. F., Hassanizadeh, S. M., & de Bruin, R. H. A. M. (2002). Two-site kinetic modeling of bacteriophages transport through columns of saturated dune sand. *Journal of Contaminant Hydrology*, *57*(3), 259–279. https://doi.org/10.1016/s0169-7722(01)00215-7

Schijven, J. F., Sadeghi, G., & Hassanizadeh, S. M. (2016). Long-term inactivation of bacteriophage PRD1 as a function of temperature, pH, sodium and calcium concentration. *Water Research*, *103*, 66–73. https://doi.org/10.1016/j.watres.2016.07.010

Schijven, J. F., van den Berg, H. H. J. L., Colin, M., Dullemont, Y., Hijnen, W. A. M., Magic-Knezev, A., et al. (2013). A mathematical model for removal of human pathogenic viruses and bacteria by slow sand filtration under variable operational conditions. *Water Research*, *47*(7), 2592–2602. https://doi.org/10.1016/j.watres.2013.02.027

Schmid-Hempel, P., & Frank, S. A. (2007). Pathogenesis, virulence, and infective dose. *PLoS Pathogens*, *3*(10), e147. https://doi.org/10.1371/journal.ppat.0030147

Schubert, J. (2002). Hydraulic aspects of riverbank filtration-field studies. *Journal of Hydrology*, *266*(3), 145–161. https://doi.org/10.1016/s0022-1694(02)00159-2

Sharma, L., Greskowiak, J., Ray, C., Eckert, P., & Prommer, H. (2012). Elucidating temperature effects on seasonal variations of biogeochemical turnover rates during riverbank filtration. *Journal of Hydrology*, *428–429*(429), 104–115. https://doi.org/10.1016/j.jhydrol.2012.01.028

Shen, C., Li, B., Huang, Y., & Jin, Y. (2007). Kinetics of coupled primary- and secondary-minimum deposition of colloids under unfavorable chemical conditions. *Environmental Science & Technology*, *41*(20), 6976–6982. https://doi.org/10.1021/es070210c

Sochala, P., & Le Maître, O. P. (2013). Polynomial chaos expansion for subsurface flows with uncertain soil parameters. *Advances in Water Resources*, *62*, 139–154. https://doi.org/10.1016/j.advwatres.2013.10.003

Sprenger, C., Lorenzen, G., Grunert, A., Ronghang, M., Dizer, H., Selinka, H.-C., et al. (2014). Removal of indigenous coliphages and enteric viruses during riverbank filtration from highly polluted river water in Delhi (India). *Journal of Water and Health*, *12*(2), 332–342. https://doi.org/10.2166/wh.2014.134

Stauffer, F., Bayer, P., Blum, P., Giraldo, N. M., & Kinzelbach, W. (2013). *Thermal use of shallow groundwater*. CRC Press.

Syngouna, V. I., & Chrysikopoulos, C. V. (2015). Experimental investigation of virus and clay particles cotransport in partially saturated columns packed with glass beads. *Journal of Colloid and Interface Science*, *440*, 140–150. https://doi.org/10.1016/j.jcis.2014.10.066

Tufenkji, N., & Elimelech, M. (2004). Deviation from the classical colloid filtration theory in the presence of repulsive DLVO interactions. *Langmuir*, *20*(25), 10818–10828. https://doi.org/10.1021/la0486638

Wang, Y., Bradford, S. A., & Šimůnek, J. (2013). Transport and fate of microorganisms in soils with preferential flow under different solution chemistry conditions. *Water Resources Research*, *49*(5), 2424–2436. https://doi.org/10.1002/wrcr.20174

Weaver, L., Sinton, L. W., Pang, L., Dann, R., & Close, M. (2013). Transport of microbial tracers in clean and organically contaminated silica sand in laboratory columns compared with their transport in the field. *Science of The Total Environment*, *443*, 55–64. https://doi.org/10.1016/j.scitotenv.2012.09.049

Wielen, P. W. J. J. v. d., Senden, W. J. M. K., & Medema, G. (2008). Removal of bacteriophages MS2 and ΦX174 during transport in a sandy anoxic aquifer. *Environmental Science & Technology*, *42*(12), 4589–4594. https://doi.org/10.1021/es800156c

World Health Organization (WHO). (2017). *Guidelines for drinking-water quality* (4th ed.). Geneva.

Xagoraraki, I., Yin, Z., & Svambayev, Z. (2014). Fate of viruses in water systems. *Journal of Environmental Engineering*, *140*(7), 04014020. https://doi.org/10.1061/(asce)ee.1943-7870.0000827

Zhou, D., Zhang, Y., Gianni, G., Lichtner, P., & Engelhardt, I. (2018). Numerical modelling of stream-aquifer interaction: Quantifying the impact of transient streambed permeability and aquifer heterogeneity. *Hydrological Processes*, *32*(14), 2279–2292. https://doi.org/10.1002/hyp.13169